



The description and validation of the computationally Efficient CH₄–CO–OH (ECCOHv1.01) chemistry module for 3-D model applications

Yasin F. Elshorbany^{1,2}, Bryan N. Duncan¹, Sarah A. Strode^{1,3}, James S. Wang^{1,3}, and Jules Kouatchou^{1,4}

¹NASA Goddard Space Flight Center, Greenbelt, Maryland, USA

²Earth System Science Interdisciplinary Center, University of Maryland, College Park, Maryland, USA

³Universities Space Research Association, Columbia, Maryland, USA

⁴Science Systems and Applications Inc., Lanham, Maryland, USA

Correspondence to: Yasin F. Elshorbany (yasin.f.elshorbany@nasa.gov)

Received: 28 September 2015 – Published in Geosci. Model Dev. Discuss.: 2 November 2015

Revised: 1 February 2016 – Accepted: 10 February 2016 – Published: 26 February 2016

Abstract. We present the Efficient CH₄–CO–OH (ECCOH) chemistry module that allows for the simulation of the methane, carbon monoxide, and hydroxyl radical (CH₄–CO–OH) system, within a chemistry climate model, carbon cycle model, or Earth system model. The computational efficiency of the module allows many multi-decadal sensitivity simulations of the CH₄–CO–OH system, which primarily determines the global atmospheric oxidizing capacity. This capability is important for capturing the nonlinear feedbacks of the CH₄–CO–OH system and understanding the perturbations to methane, CO, and OH, and the concomitant impacts on climate. We implemented the ECCOH chemistry module in the NASA GEOS-5 atmospheric global circulation model (AGCM), performed multiple sensitivity simulations of the CH₄–CO–OH system over 2 decades, and evaluated the model output with surface and satellite data sets of methane and CO. The favorable comparison of output from the ECCOH chemistry module (as configured in the GEOS-5 AGCM) with observations demonstrates the fidelity of the module for use in scientific research.

1 Introduction

The coupled methane–carbon monoxide–hydroxyl radical (CH₄–CO–OH) system is nonlinear (e.g., Prather, 1994) and important in determining the atmosphere's oxidizing capacity (e.g., Chameides et al., 1976). Methane is the sec-

ond most important anthropogenic greenhouse gas (GHG), though its 100-year global warming potential (GWP) is 34 times larger than that of carbon dioxide (CO₂; Myhre et al., 2013). Methane is responsible for about 20 % of the warming induced by long-lived GHGs since pre-industrial times (Kirschke et al., 2013). The CH₄–CO–OH system has implications for tropospheric ozone and, subsequently, air quality (e.g., Fiore et al., 2002). A thorough understanding of historical methane, CO, and OH trends and variations is necessary to credibly predict future changes and their climate feedback, as well as to develop strategic national and international emission reduction policies.

The major limitation of forward modeling studies of trends and variability in the CH₄–CO–OH system is the computational expense associated with simulating ozone–nitrogen oxides–volatile organic compounds (O₃–NO_x–VOC) photochemistry for the determination of OH, particularly since perturbations to relatively long-lived methane (~8–10 years) can take several decades to fully evolve (e.g., Prather, 1996). There are few forward modeling studies in the literature that carry a full representation of O₃–NO_x–VOC chemistry, and they necessarily present a limited number of sensitivity simulations (e.g., Fiore et al., 2006; Voulgarakis et al., 2015).

To overcome this computational expense, global modeling communities often use archived and annually repeating monthly OH fields to simulate the oxidation of methane and CO. In the TransCom methane model intercomparison project (MIP), archived and annually repeating OH fields

were used from a climatology (Spivakovsky et al., 2000). Wang et al. (2004) used archived and annually varying OH fields from Duncan et al. (2007a) to explain the causes of observed interannual variations in methane and the observed slowdown in its growth rate from 1988 to 1997.

Limitations of using archived, monthly OH fields for studies of methane's and CO's evolution are that feedbacks of the CH₄–CO–OH system on methane, CO, and OH are not captured as the losses of methane and CO by reaction with OH are assumed to be linearly proportional to the OH fields. For methane, this assumption is not desirable, particularly on multi-decadal timescales (e.g., Prather, 1996). Chen and Prinn (2006) found that using an archived, annual cycle of OH may mask or bias the interannual changes of methane. For relatively short-lived CO (~1–2 months), this assumption is not valid given the strong feedback between CO and OH (e.g., Duncan and Logan, 2008; Voulgarakis et al., 2015). If a multi-decadal simulation of methane or CO using archived and annually repeating OH reproduces observations, then there must be some compensating factor, for example, a bias in emissions. That is, the simulation reproduces observations, but for the wrong reason. The models in the TranCom MIP adjusted down (by 8%) the archived OH climatology of Spivakovsky et al. (2000) so that the simulated decline in the global, atmospheric methylchloroform (MCF) concentration since 2000 better matched that observed (Patra et al., 2011). Adjusting archived OH to improve a simulation of MCF, methane, and/or CO makes the specious assumption that emissions inventories, model dynamics, etc., used in the simulation are correct. When using archived and annually repeating OH, whether adjusted or not, inverse modeling studies of methane and CO will incorrectly determine a posteriori fluxes as the impact of nonlinear feedbacks of the CH₄–CO–OH system on concentrations will be erroneously folded into the flux estimates. Therefore, there is a need for a computationally efficient solution to simulate credible temporal and spatial distributions of OH over several decades, while capturing the nonlinear feedbacks of the CH₄–CO–OH system.

In this paper, we present and validate the new, computationally Efficient CH₄–CO–OH (ECCOH; pronounced “echo”) chemistry module to interactively simulate the chemistry of the CH₄–CO–OH system within a chemistry-climate model, carbon cycle model, or Earth system model. The computational efficiency of the ECCOH chemistry module allows many sensitivity simulations of multiple decades to be performed, which is important for capturing the nonlinear feedbacks of the CH₄–CO–OH system and understanding the perturbations to methane and the concomitant impacts on climate. The ECCOH chemistry module allows one to deconvolve the impacts of various causal factors (e.g., overhead ozone column, NO_x, VOCs, water vapor) on OH and, subsequently, on methane and CO. Therefore, this capability is valuable in determining these impacts, especially given that simulated OH varies widely between models (Shindell et al., 2006; Fiore et al., 2009) for a variety of reasons, in-

cluding differences in the causal factors that influence OH (Shindell et al., 2006). For instance, Voulgarakis et al. (2013) found that simulated tropospheric methane lifetimes of various models ranged from ~7 to ~14 years; this spread is similar to that calculated by Shindell et al. (2006) and Fiore et al. (2009), even when all participating models used identical methane abundances and CO emissions (Shindell et al., 2006). Shindell et al. (2006) related the wide spread of simulated CO between models to the wide spread of simulated OH. Furthermore, simulated OH from full chemistry mechanisms in global models is still highly uncertain because of incomplete knowledge and representation of OH sources, sinks, and recycling (e.g., Elshorbany et al., 2010, 2012a, b, 2014; Stone et al., 2012). For example, (1) nitrous acid (HONO) is typically underestimated in models by an order of magnitude (Elshorbany et al., 2012b), which can lead to a significant underestimation of OH, especially in urban high-NO_x regions; (2) in unpolluted, forested environments, significant discrepancies exist between models and measurements (Stone et al., 2012); and (3) Patra et al. (2014) indicate that the inter-hemispheric OH ratio (Northern to Southern Hemisphere) is near unity, while a recent model intercomparison had a multi-model average of about 1.3.

The paper is organized as follows: in Sect. 2, we (1) describe the ECCOH chemistry module as implemented in the NASA Goddard Earth Observing System, Version 5 atmospheric general circulation model (GEOS-5 AGCM), and (2) describe a series of simulations, which we refer to as “scenarios” hereafter, to illustrate the utility of the ECCOH module for understanding the influence of various factors on the observed spatial distributions and temporal evolution of methane, CO, and OH. In Sect. 3, we show that the simulated trends and variations of methane and CO in our reference scenario agree well with in situ and satellite measurements. In Sect. 4, we demonstrate the ability of the ECCOH chemistry module to capture the nonlinear chemistry of the CH₄–CO–OH system with output from our sensitivity scenarios.

2 Technical approach and methodology

2.1 Description of the ECCOH chemistry module and its implementation

The ECCOH chemistry module is composed of a parameterization of tropospheric OH and tracers of methane and CO as shown in Fig. 1. The advantage of the ECCOH chemistry module over a full representation of O₃–NO_x–VOC chemistry is computational efficiency. The computational cost of simulating tropospheric OH is reduced by a factor of about 500 when the full O₃–NO_x–VOC chemistry is replaced by the parameterization of OH (Duncan et al., 2000). This computationally efficient parameterization of OH allows (1) for many multi-decadal model sensitivity simulations to be performed and (2) one to deconvolve the impact of various fac-

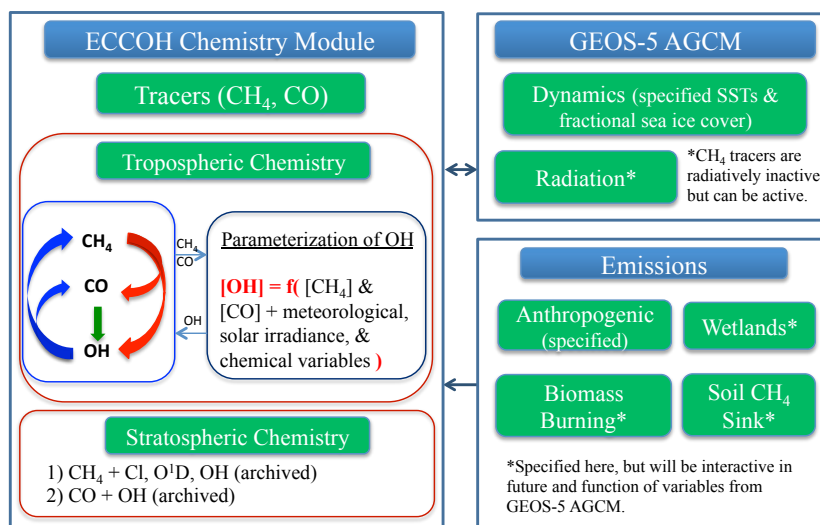


Figure 1. Schematic representation of the implementation of the ECCOH module within the GEOS-5 AGCM.

tors on the observed trends and variability in methane and CO. It is based on the method described by Spivakovsky et al. (1990a), who developed an earlier version of the parameterization of OH used in several studies, including Spivakovsky et al. (1990b) and Prather and Spivakovsky (1990). The parameterization of OH of Duncan et al. (2000) is designed to simulate OH over the range of photochemical environments found throughout the troposphere, including a wide enough range so as to be applicable to preindustrial, present-day and possible future conditions (Duncan et al., 2000). It has been implemented in two host atmospheric models and has been used in several studies of the nonlinear feedbacks of CO and OH (Duncan et al., 2007a; Duncan and Logan, 2008; Strode et al., 2015).

The parameterization of OH accurately represents OH predicted by a full chemical mechanism as a set of high-order polynomials that describe the functional relationship between the concentration of OH and meteorological variables (i.e., pressure, temperature, cloud albedo), solar irradiance variables (i.e., ozone column, surface albedo, declination angle, latitude), and chemical variables, including CO and methane as well as nitrogen oxides (as a family), ozone, water vapor, and various VOCs. That is, the 24 h average OH is calculated interactively in the model and responds to changes in the concentrations of trace gases and meteorology. Input variables to the parameterization of OH may be taken from archived fields from, for instance, an observational climatology or archived fields from a model simulation with a full representation of trace gas and aerosol atmospheric chemistry, and may be annually repeating or annually varying. Some variables (e.g., water vapor, clouds) may be taken from the host model as the simulation progresses. Ideally, all input variables should be annually varying so as to best capture the nonlinear feedbacks of the CH₄–CO–OH

system. If one chooses to use output from a single computationally expensive full chemistry model simulation as input to the parameterization of OH, subsequent sensitivity simulations using the ECCOH chemistry module will be far less computationally expensive relative to that single expensive simulation, which is the primary strength of using the parameterization of OH. In Sect. 2.2, we discuss the setup of the simulations presented in this study.

We adjust the OH from the parameterization to account for important updates in kinetic information of O¹D reactions by water vapor, molecular nitrogen, and molecular oxygen (Sander et al., 2011). These reactions are key as the primary production pathway (*P*) for OH involves the formation of excited O¹D atoms by photolysis of ozone (O₃), followed by their reaction with water vapor in competition with their collisional quenching by molecular nitrogen and oxygen: $P = j[\text{O}_3] \cdot 2k_1[\text{H}_2\text{O}]/(k_1[\text{H}_2\text{O}] + k_2[\text{N}_2] + k_3[\text{O}_2])$, where *j* is the ozone photolysis rate and *k*₁, *k*₂, and *k*₃ are the rate constants of O¹D reactions with water vapor, nitrogen, and oxygen, respectively. Typically, this adjustment decreases OH by 10–30 %, depending on altitude and season. Recent updates in isoprene chemistry are not reflected in the parameterization of OH, so OH near the surface in clean, forested environments (e.g., the Amazon and Congo basins) is too low relative to current knowledge (e.g., Fuchs et al., 2013). However, the contribution of these regions to global methane and CO loss is small (i.e., < 1 %), and the current knowledge of isoprene photochemistry is still highly uncertain (Fuchs et al., 2013). Ultimately, the parameterization of OH reflects uncertainties in the chemistry upon which it is based, as do the photochemical mechanisms in all atmospheric chemistry models (e.g., Stone et al., 2012; Fuchs et al., 2013). The losses of methane and CO in the ECCOH chemistry module are determined by their reaction with tro-

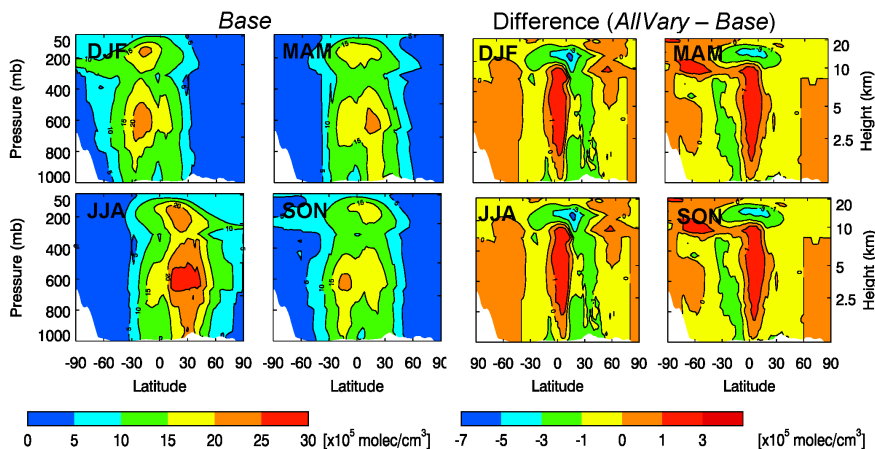


Figure 2. Seasonal zonal mean (1988–2007) of OH ($\times 10^5$ molecules cm^{-3}) for the *Base* scenario (left four panels) and the difference (*AllVary*–*Base*, right four panels) for December–February (DJF), March–May (MAM), June–August (JJA), and September–November (SON).

ospheric OH. Additional losses of methane in the stratosphere occur by reactions with OH, Cl, and O¹D, whose distributions are simulated using archived and annually repeating monthly fields.

We implemented the ECCOH chemistry module in the Goddard Earth Observing System, Version 5 atmospheric general circulation model (GEOS-5 AGCM, Fortuna version, Rienecker et al., 2008; Pawson et al., 2008; Ott et al., 2010; Molod et al., 2012). The AGCM combines the finite-volume dynamical core described by Lin (2004) with the GEOS-5 column physics package, as summarized by Rienecker et al. (2008). The AGCM domain extends from the surface to 0.01 mb and uses 72 hybrid layers that transition from terrain following near the surface to pure pressure levels above 180 mb. We use a horizontal resolution of 2° latitude \times 2.5° longitude and the time step is 30 min for physical computations.

2.2 Description of the reference and sensitivity scenarios

To demonstrate the utility of the ECCOH chemistry module for multi-decadal studies, we performed several model simulations using the module in the GEOS-5 AGCM (Tables 1 and 2). The model setup (i.e., emissions, input to the parameterization of OH, and dynamics) of the reference scenario, which we refer to as the *Base* scenario, is detailed in Table 1. Compared to the sensitivity scenarios described in Table 2, the *Base* scenario is the least complex. For example, all CO emissions and natural methane emissions are for 1 year that are repeated for each year of the simulation (1988–2007); therefore, interannual variations in methane and CO levels caused by variations in these emissions will not be captured in the *Base* scenario. However, there are two important sources of variability that are included in the *Base* scenario.

First, the dynamics are constrained by varying sea surface temperatures and sea ice concentrations. Therefore, the *Base* scenario will capture variations in methane, CO, and OH resulting from meteorological variations, such as those associated with the El Niño–Southern Oscillation (ENSO). In addition, atmospheric temperature, pressure, and specific humidity are calculated online by the GEOS-5 AGCM and are fed into the parameterization of OH as the runs progress, so interannual variations in water vapor, temperature, and cloud cover are also included in the *Base* scenario. These factors are known to influence variations in OH and thus CO and methane (e.g., Holmes et al., 2013). Second, interannual variations in anthropogenic methane sources are included in the *Base* scenario. In Sect. 3, we evaluate model output from the *Base* scenario with the observational data sets described in Table 3.

We present the results of our sensitivity scenarios in Sect. 4. We explore the influence of several causal factors on the observed spatial distributions and temporal evolutions of methane, CO, and OH. These causal factors include annually varying methane and CO emissions (i.e., Scenarios 2–4: Table 2; natural methane emissions, and anthropogenic and natural CO emissions: Figs. S1 and S2 in the Supplement) and annually varying input variables to the parameterization of OH (i.e., Scenario 5 in Table 2).

3 Evaluation of the *Base* scenario

We evaluate the model output of methane and CO from the *Base* scenario with satellite and in situ observations (Table 3). We also compare simulated OH with that from a GEOS-5 AGCM simulation (with a full representation of O₃–NO_x–VOC chemistry (Strode et al., 2015)). We highlight where the *Base* scenario’s simplicity results in a poor or satisfac-

Table 1. Reference scenario (*Base*) description.

AGCM Input	Description ^a
Dynamics	Model dynamics are constrained by sea surface temperatures and sea ice concentrations from the Community Climate System Model (http://www.cesm.ucar.edu/models/ccsm4.0/ , CCSM-4) through 2005 and from 2006 to 2007 from CCSM-4 with a Representative Concentration Pathway (RCP 6.0, Fujino et al., 2006; Hijioaka et al., 2008). The methane tracer is radiatively inactive and archived annually varying methane fields used in the radiation code; our aim is reproduce the same meteorology in all simulations so as to more cleanly isolate the impact of the causal factors on methane, CO, and OH trends and variations.
Parameterization of OH input	
Chemical variables	Nitrogen oxides (as a family), ozone, overhead ozone column, and various VOCs are monthly, archived fields for 2000 and are repeated for each year of the <i>Base</i> simulation; these fields were taken from a 1-year (2000) GEOS-5 AGCM simulation, which was part of the ACCMIP study (Lamarque et al., 2013), with a full representation of ozone–NO _x –VOC photochemistry (Duncan et al., 2007b; Strahan et al., 2007) and emissions of NO _x , VOCs, and species important to the stratospheric ozone layer (e.g., N ₂ O, HFCs, CFCs).
Meteorological variables	Pressure, temperature, cloud albedo and water vapor are taken from the AGCM as the simulation progresses.
Emissions ^b	
Methane	Annually repeating natural (e.g., wetlands, biomass burning) and annually varying anthropogenic emissions (EDGAR 3.2, TransCom CTL scenario) are described in Patra et al. (2011).
CO	Annually repeating emissions representative for the year 2000 time slice of the ACCMIP (Lamarque et al., 2013; Strode et al., 2015).
Methane oxidation	
Troposphere	CH ₄ + OH → αCO: tropospheric OH calculated by parameterization of OH. CO yield (α) = 1 (Duncan et al., 2007a).
Stratosphere	Calculated based on its reaction with OH, Cl and O ¹ D from archived monthly fields from 1 year of an AGCM simulation.
VOC oxidation ^b	VOC + OH → α CO; CO yield (α) varies with VOC (Duncan et al., 2007b). Isoprene + OH → α CO, where CO yield (α) varies with [NO _x] (Duncan et al., 2007a).

^a All scenarios are for 1988–2007. We use the methane initial condition of 1655 ppb by January 1988 at the GMD South Pole (SPO) station, (Patra et al., 2011, TransCom protocolv7), which was reached after a 12-year model spin-up; results are thus considered valid from 1 January 1988. ^b Only methane and CO are treated as emission fluxes. The source of CO via VOC oxidation is calculated using archived, 3-D fields from a GEOS-5 AGCM full chemistry simulation. Figures S1 and S2 show the methane and CO fluxes, respectively, used in all scenarios.

tory comparison of the model output with the observed temporal and spatial distributions of methane, CO, and OH. We demonstrate that the ECCOH chemistry module for this scenario reasonably captures the distributions of methane and CO, within the limitations of this scenario, as compared to measurements and other model studies (e.g., Shindell et al., 2006; Patra et al., 2011; Naik et al., 2013).

3.1 Tropospheric OH

There are very few direct observations of OH with which to constrain models (e.g., Stone et al., 2012), and none on regional or global scales. Therefore, the MCF lifetime inferred from measurements serves as a widely used, indirect proxy for global OH abundance (e.g., Lawrence et al., 2001). Though useful, the MCF lifetime gives an incomplete description of the spatial and vertical distributions of OH (e.g.,

Lawrence et al., 2001), and there are uncertainties concerning MCF emissions and the resulting lifetime estimate (e.g., Wang et al., 2008). Nevertheless, the MCF data have been recently used to infer the ratio of OH in the Northern to Southern Hemisphere (Patra et al., 2014).

Despite the challenges concerning OH, we show in this section that the spatial and vertical distributions of simulated global mean OH (Figs. 2 and 3) from the *Base* scenario are reasonable relative to the MCF proxy for OH as well as to simulated OH from other models. Related to the OH dependency on UV radiation (Rohrer and Berresheim, 2006), the maximum and minimum OH levels at any given location occur in local summer and winter, respectively (Fig. 2). OH maximizes around 600 mb because of vertical dependencies of the main sources and sinks of OH (Spivakovsky et al., 1990). The seasonal and vertical distributions of the zonal mean OH in the *Base* scenario are comparable to the OH

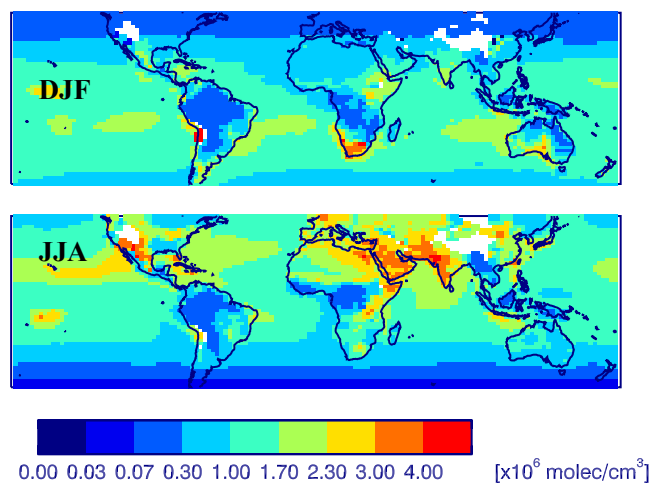
Table 2. Description of simulation scenarios.

Model scenario	Relation to other scenarios	Purpose of scenario
<i>Base</i>	Table 1	Reference scenario
<i>E</i> CH ₄ <i>Vary</i> <i>Base</i> + all methane source types varying annually	Same as <i>Base</i> , except that the “EXTRA” methane emission scenario is used (Patra et al., 2011). The primary difference between the CTL and EXTRA scenarios is that the CTL emissions are composed of repeating annual cycles of all source types, except for anthropogenic emissions that vary from year to year, while the EXTRA emission scenario has all source types (e.g., biomass burning, wetlands, rice paddies) varying annually (Fig. S1).	To understand the influence of interannual variations in natural sources of methane on the trends and variations of model OH and observed methane and CO distributions. Wetlands are the largest single source of methane and the largest source of interannual variations (e.g., Patra et al., 2011; Youlgarakis et al., 2015).
<i>BB</i> CO <i>Vary</i> <i>Base</i> + <i>BB</i> CO emissions varying annually	Same as <i>Base</i> , except that CO emissions from biomass burning (<i>BB</i>) vary annually. Emissions are from the REanalysis of the TROPOspheric chemical composition (RETRO v2.0, Schultz et al., 2007) emission inventory for 1988–1996 and the Global Fire Emissions Database (GFEDv3.1, Giglio et al., 2010; Randerson et al., 2013) for years 1997–2007.	To understand the influence of interannual variations in the biomass burning source of CO (Fig. S2). From 1988 to 2007, there were several large events, such as in Indonesia in 1997 (Duncan et al., 2003a) and 2006 and worldwide in 1998 (Duncan et al., 2003b).
<i>FFBB</i> CO <i>Vary</i> <i>Base</i> + FF and BB CO emissions varying annually	Same as <i>BB</i> CO <i>Vary</i> , except that CO emissions from fossil fuels vary annually. Anthropogenic emissions are from the Emission Database for Global Atmospheric Research (EDGARv4.2) for 1988–2007.	To understand the combined influence of interannual variations in the anthropogenic and biomass burning sources of CO.
OH _{Input} <i>Vary</i> <i>Base</i> + parameterization of OH chemical variables varying annually	Same as <i>Base</i> , except the monthly, archived chemical variables used as input to the parameterization of OH are annually varying. Taken from the same GEOS-5 AGCM simulation as in <i>Base</i> scenario with a full representation of ozone–NO _x –VOC photochemistry and annually varying anthropogenic and biogenic emissions of NO _x , VOCs, and species important to the stratospheric ozone layer (e.g., N ₂ O, HFCs, CFCs) (Strahan et al., 2007; Duncan et al., 2007b; Oman et al., 2011).	To understand the influence of interannual variations in other factors that affect OH. These factors include the overhead ozone column, NO _x and anthropogenic VOCs.
All <i>Vary</i> <i>Base</i> + <i>E</i> CH ₄ <i>Vary</i> + <i>FFBB</i> CO <i>Vary</i> + <i>OH</i> _{Input} <i>Vary</i>	Annually varying methane and CO emissions from all sources and annually varying factors that influence OH.	To understand the combined influence of annually varying (1) CO emissions from fossil fuel and biomass burning, (2) effects of NO _x and VOCs on OH, and (3) methane emissions from all sources.

Table 3. Data used in model evaluation of methane, CO, and OH.

Data	Species	Quantity	Time range	Reference
NOAA ESRL Global Monitoring Division (GMD) surface data	CO, methane	Mixing ratio (ppbv)	1980–present	Novelli et al. (1992, 1998), Dlugokencky et al. (2010, 2014)
Envisat Scanning Imaging Absorption spectroMeter for Atmospheric CHartograph Y (SCIAMACHY) ^a	Methane	Atmospheric (molec cm ⁻²)	2003–2005	Bovensmann et al. (1999), Schneising et al. (2009, 2011), Frankenberg et al. (2011)
Terra Measurement of Pollution In The Troposphere (MOPITT) instrument ^b	CO	Atmospheric (molec cm ⁻²)	1999–present	Worden (2010), Deeter et al. (2012), Deeter (2013)
Aura Tropospheric Emission Spectrometer (TES)/Microwave Limb Sounder (MLS) joint product	CO	Mixing ratio (ppbv)	8/2004–10/2012	Luo et al. (2013)
NOAA surface network	MCF	OH interannual variability (IAV) ^c	1997–2007	Montzka et al. (2011)

^a We use the version 3.7 gridded product of the column-averaged methane dry mole fraction (Schneising et al., 2009; http://www.iup.uni-bremen.de/sciamachy/NIR_NADIR_WFM_DOAS_products). The methane data since November 2005 are considered to be of reduced quality (in comparison to data from 2003 to October 2005) due to detector degradation in the spectral range used for the methane column retrieval (Schneising et al., 2011; Frankenberg et al., 2011). ^b We use the gridded monthly CO retrievals (thermal infrared radiances) V006 L3 product (<http://eosweb.larc.nasa.gov>). ^c There are only very sparse and uncertain direct observations (e.g., Stone et al., 2012).

**Figure 3.** Seasonal mean (1988–2007) OH ($\times 10^6$ molecules cm^{-3}) for the *Base* scenario for December–February (DJF) and June–August (JJA) at 850 mbar.

climatology of Spivakovsky et al. (2000; see Fig. 6 of Spivakovsky et al., 1990), despite the different inputs given to the parameterization of OH in the two studies.

The interannual variations in global OH (given by the annual mean standard deviation, not shown) are small ($< 5\%$) and mainly related to meteorological variations (e.g., water vapor, clouds, temperature, and transport) as annually repeating emissions are used in the *Base* scenario, except for anthropogenic methane emissions (Table 1, Fig. S1). This result is consistent with Voulgarakis et al. (2013), who show that OH has the strongest relationship with changes in temperature and humidity when emissions do not vary interannually. As discussed in Sect. 4, we see considerably larger variations in OH in several of our more complex sensitivity simulations, which have interannual variations in methane and CO emissions as well as in factors that affect OH.

Over our simulation period, the range of annual mean, atmospheric MCF lifetimes is 6.08 ± 0.60 to 6.53 ± 0.65 years with respect to loss by reaction with tropospheric OH for the *Base* scenario, assuming a MCF uniform mixing ratio. Our lifetimes are similar to values reported in the literature (e.g., $6.0^{+0.5}_{-0.4}$ years (Prinn et al., 2005); multi-model mean of 5.7 ± 0.9 years (Naik et al., 2013); 6.3 ± 0.9 years (Prather et al., 2012)). The global, annual mean lifetime of methane with respect to tropospheric OH ranges from 10.10 ± 1.06 to 10.86 ± 1.15 years. These values are similar to those inferred from measurements (e.g., $10.2^{+0.9}_{-0.7}$ years (Prinn et al., 2005)) as well as to those reported in previous multi-model comparison studies (e.g., 9.7 ± 1.7 years (Shindell et al., 2006); 10.19 ± 1.72 years (Fiore et al., 2009); 9.7 ± 1.5 years (Naik et al., 2013)). The lifetime of methane is calculated by dividing the total atmospheric burden by the tropospheric methane loss rate (e.g., Fiore et al., 2009).

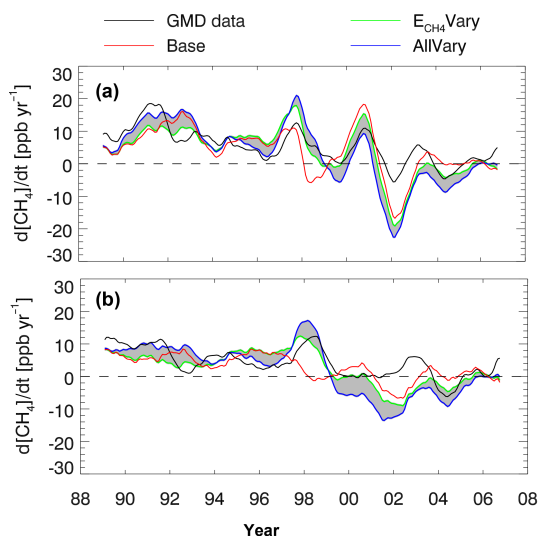


Figure 4. (a) Twelve-month running mean atmospheric growth rate of methane (ppbv yr^{-1}) for the average of 92 GMD stations and from model output for several scenarios averaged for those station locations. The shaded area is the difference between the E_{CH_4} Vary and AllVary scenarios, which indicates the total contribution of non-linear feedbacks (i.e., from variations of CO emissions and variables input to the parameterization of OH) of the CH₄–CO–OH system to methane’s growth rate. (b) Same as (a) but for the average of 17 GMD stations, which covers 100 % of the simulation period. Refer to Figs. S4 to S7 for methane’s growth rate from other scenarios.

We also compare our simulated OH with that from a GEOS-5 AGCM simulation that carries a full representation of O₃–NO_x–VOC chemistry. This simulation was included in the Atmospheric Chemistry and Climate Model Intercomparison Project (ACCMIP, Lamarque et al., 2013; the model is designated as “GEOSCCM”). Henceforth, we refer to this simulation as the “ACCMIP simulation”. The same CO emissions (annually repeating emissions for the year 2000) are used in both the Base and ACCMIP simulations, but there are differences between the simulations (e.g., model dynamics, prescribed methane). Despite these differences, we find that the spatial and vertical distributions of OH are quite similar, with differences generally less than 10 % (Fig. S17). The global, mean tropospheric OH in the Base scenario of 10.9×10^5 molecules cm^{-3} also compares well with that of 11.4×10^5 molecules cm^{-3} from the ACCMIP simulation (the 2000 time slice) as well as within the range of means from other models (e.g., 6.5 – 13.4×10^5 molecules cm^{-3} (Voulgarakis et al., 2013)).

3.2 Methane

GMD surface data. We evaluate our simulated surface distributions of methane with data from the NOAA Global Monitoring Division (GMD) network. The simulated, interannual variation of methane’s global growth rate agrees reasonably

well ($R^2 = 0.44$) with that estimated from GMD data, using all available data from 92 stations over the simulation period 1988–2007 (Fig. 4a). The agreement of model output with observations is worse ($R^2 = 0.33$) when we only use the 17 stations that cover the entire simulation period (Fig. 4b). We decided to include all 92 stations, even those without records that cover the entire simulation period, as we are able to nearly reproduce Fig. 4a using 46 stations that have at least 75 % data coverage (not shown). A relatively high correlation coefficient ($R^2 = 0.44$) implies that interannual variations in anthropogenic methane emissions and dynamics explain much of methane’s growth rate over the study period, which is consistent with the findings of the TransCom MIP (Patra et al., 2011).

Overall, the comparison of model output and data at individual GMD stations is favorable. Figures 5 to 7 show comparisons for monthly averages, seasonal averages, and annual differences, respectively, at six GMD stations, which were chosen as they have long time records and cover a wide range of latitudes. Over the simulation period (1988–2007), the correlation slope (S) and coefficient (R^2) for these six stations (Table 4) range from 0.56 to 0.79 and from 0.58 to 0.91, respectively.

There are two important features of the observations that are not simulated in the Base scenario. First, the Base scenario overestimates methane concentrations by 20–30 ppbv at the northern high-latitude stations of Alert and Barrow during the 1980s and 1990s (Figs. 5–7). The overestimation of methane in the Northern Hemisphere during the 1990s occurs because of regional high biases in natural methane emissions (Fig. S1 and Patra et al., 2011). As shown in Sect. 4.3, simulated methane improves significantly in the Northern Hemisphere in the E_{CH_4} Vary scenario, which includes annually varying natural methane emissions. Second, the Base scenario captures the increasing observed methane trend in the 1990s, but underpredicts methane in the 2000s (Fig. 7). Both of these features (i.e., high bias at high northern latitudes in the 1990s and low bias in the 2000s) are consistent with the findings of the TransCom MIP that used the same methane emissions (Table 1 and Patra et al., 2011).

SCIAMACHY methane. We compare the simulated methane dry columns to those from SCIAMACHY (Table 3, Fig. 8). The data have the best global spatial coverage during boreal summer because of lower cloud cover during this season (Schneising et al., 2011). The observed methane dry columns reach their highest levels during boreal summer and fall, maximizing over Asia (eastern China and northern India) because of high emissions from wetlands and rice paddies. The Base scenario reproduces the spatial distribution of the data well, with a bias of $< 2\%$ over most of the globe, except over eastern Asia and the western US during boreal summer, where it is biased low but still within the measurement uncertainties (~ 7 – 10% ; Gloudemans et al., 2008; Houweling et al., 2014). Houweling et al. (2014) demonstrate that SCIAMACHY data have a seasonal bias that ranges from

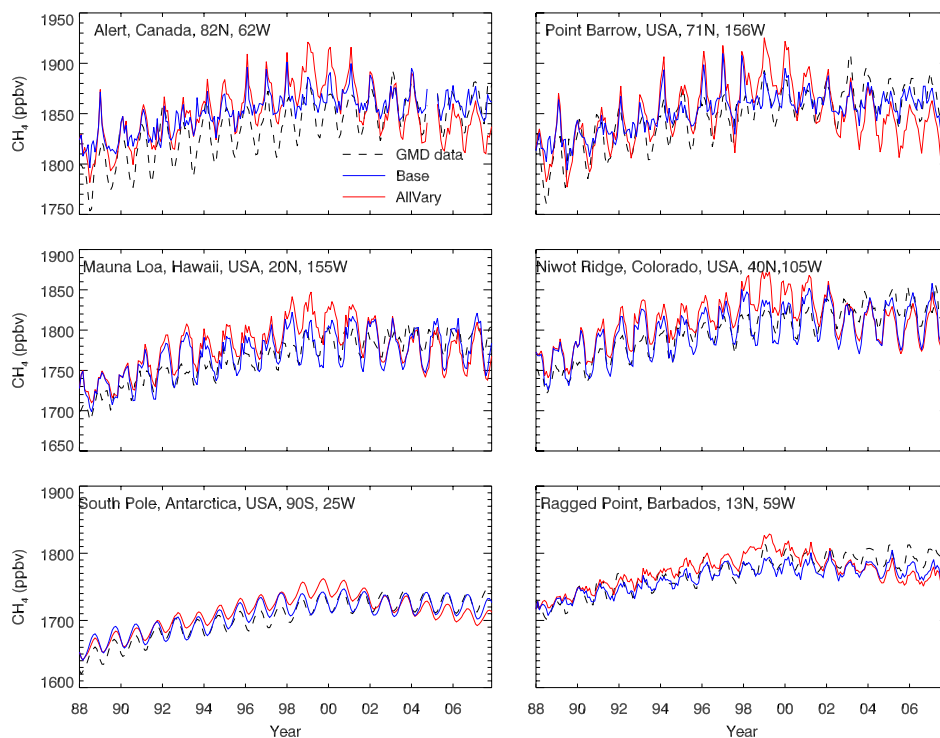


Figure 5. Monthly methane (ppbv) from the *Base* and *AllVary* scenarios and observations from six GMD stations. Similar plots for the other scenarios are given in Figs. S8 to S11.

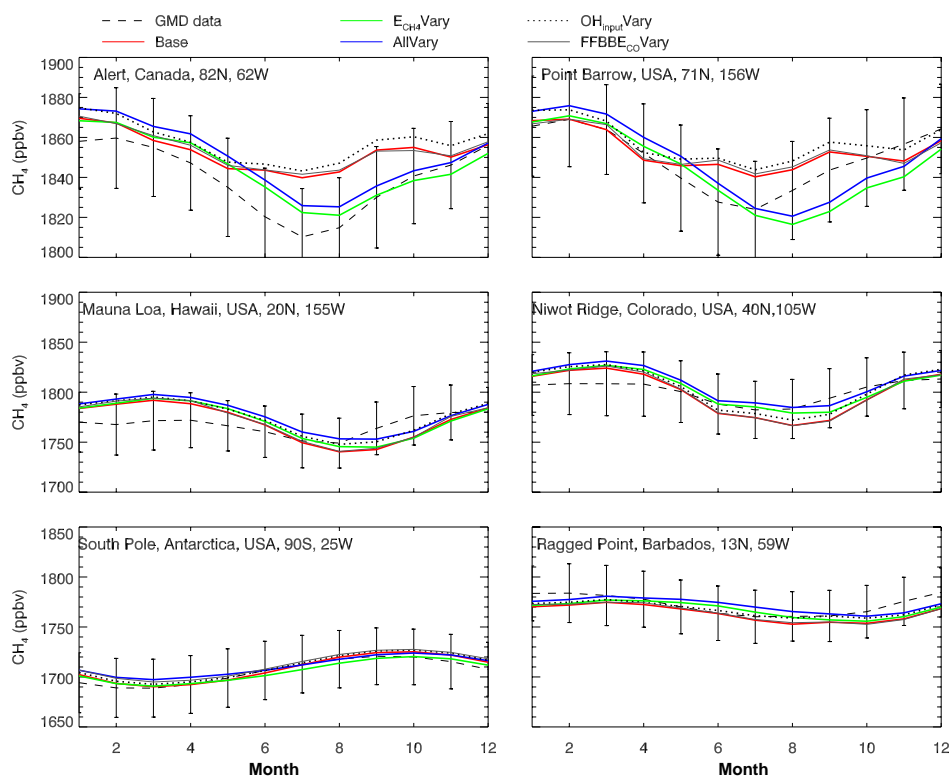


Figure 6. Monthly methane (ppbv) averaged over 1988–2007 for several scenarios and observations at six GMD stations. Vertical lines represent the standard deviation of the observed annual mean.

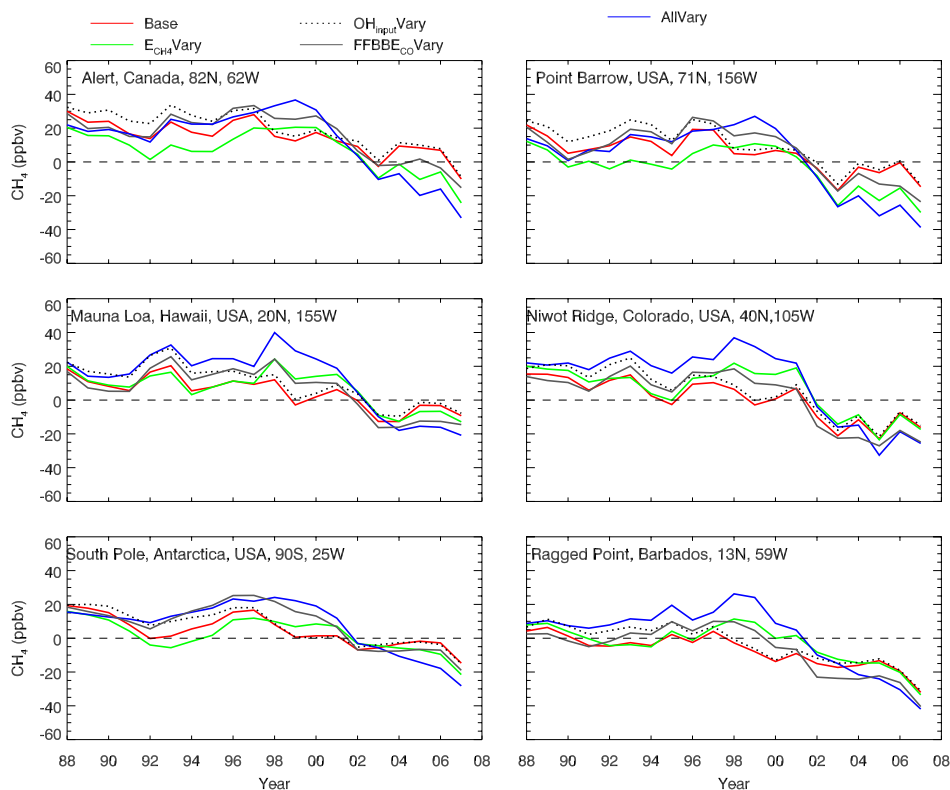


Figure 7. Annual methane deviation (ppbv; simulated–measured) for several scenarios and observations at six GMD stations.

about -50 ppb during boreal winter to about $+50$ ppb during boreal summer as compared to the Total Carbon Column Observing Network (TCCON) measurements, which may also explain the simulated seasonal biases (Fig. 8).

3.3 CO

GMD surface data. The *Base* scenario captures the monthly variability of GMD CO data well, with a mean correlation slope (S) and coefficient (R^2) of 0.81 and 0.72, respectively (Figs. 9 to 11, Table 4). This result indicates that the seasonal CO cycle is well captured in the *Base* scenario (Fig. 11), which includes annually repeating but seasonally varying biomass burning emissions (Fig. S2). As expected, the *Base* scenario does not capture the significant interannual variations associated with strong variations in emissions (Figs. 9, 10). The low biases reach ~ 40 ppb in boreal winter and spring at high northern latitudes. During the 1980s and 1990s, CO levels in the Northern Hemisphere declined substantially because of changing patterns of emissions (Duncan et al., 2007a), which is not simulated with annually repeating CO emissions. These results are in agreement with the findings of the multi-model ACCENT study (using annually repeating CO emissions), in which there was a low bias of ~ 50 ppbv at Northern Hemisphere high-latitude stations

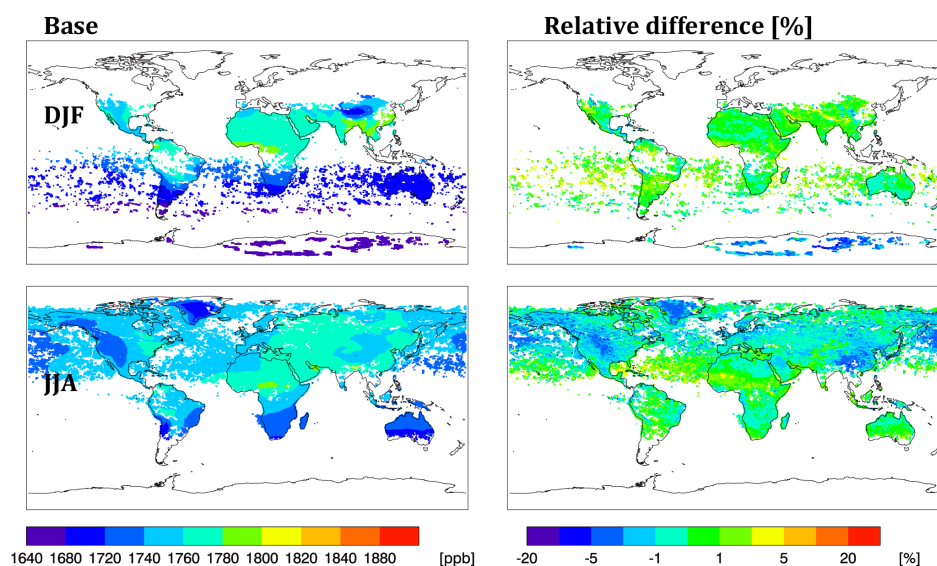
(Shindell et al., 2006), as well as with other recent studies (e.g., Monks et al., 2015).

MOPITT and TES/MLS CO. The primary advantage of satellite data, over ground-based networks, is spatial coverage, so we compare the spatial and seasonal distributions of simulated CO with those from the MOPITT and TES/MLS instruments (Figs. 12, 13). The distributions of CO from the *Base* scenario compare well overall with the data. The mean biases relative to both data sets are within $\pm 10\%$ over most of the globe and in all seasons. For example, the seasonal correlation slopes (S) range from 0.75 to 0.98 and coefficients (R^2) range from 0.80 to 0.98, respectively, between MOPITT, TES/MLS data, and the *Base* scenario output, with the agreement generally highest during boreal winter and lowest during boreal summer. However, the largest biases (Fig. 12) occur over (1) tropical and subtropical biomass burning regions ($\sim 20\%$) during boreal winter, indicating that either the CO emissions used in the *Base* scenario are too high or that simulated OH is too low, and (2) most of the Northern Hemisphere ($< -20\%$) during the summer season, indicating that either CO emissions are too low or that OH levels are too high, which is consistent with previous studies using similar emissions (e.g., Shindell et al., 2006; Strode et al., 2015). In addition to possible biases associated with emissions, some of the model–observation discrepancies may be associated with uncertainties in the satellite data

Table 4. List of the correlation parameters of the different model scenarios and the monthly GMD measurements for the simulation period (1988–2007).

Scenario	ALT ^a		BRW		NWR		MLO		RPB		SPO	
	S ^b	R ^{2c}	S	R ²	S	R ²	S	R ²	S	R ²	S	R ²
CH ₄ data												
<i>Base</i>	0.56	0.66	0.57	0.60	0.76	0.64	0.76	0.58	0.68	0.82	0.79	0.91
<i>E_{CH₄}</i> Vary	0.74	0.68	0.74	0.56	0.74	0.63	0.79	0.57	0.71	0.72	0.82	0.89
<i>BBE_{CO}</i> Vary	0.82	0.68	0.84	0.66	1.03	0.76	1.07	0.72	1.00	0.84	1.07	0.93
<i>FFBBE_{CO}</i> Vary	0.58	0.54	0.56	0.46	0.74	0.54	0.77	0.52	0.66	0.64	0.79	0.81
<i>OH_{input}</i> Vary	0.53	0.63	0.53	0.56	0.71	0.60	0.70	0.56	0.62	0.78	0.74	0.90
<i>AllVary</i>	0.69	0.49	0.68	0.40	0.64	0.45	0.70	0.43	0.62	0.47	0.76	0.73
CO data												
<i>Base</i>	0.74	0.79	0.70	0.75	0.83	0.57	0.98	0.71	0.74	0.68	0.88	0.82
<i>E_{CH₄}</i> Vary	0.74	0.79	0.70	0.75	0.82	0.57	0.98	0.71	0.73	0.68	0.87	0.82
<i>BBE_{CO}</i> Vary	0.81	0.86	0.74	0.73	0.84	0.57	1.01	0.74	0.82	0.68	0.79	0.64
<i>FFBBE_{CO}</i> Vary	0.92	0.88	0.97	0.87	0.84	0.42	0.89	0.70	0.83	0.70	0.81	0.63
<i>OH_{input}</i> Vary	0.74	0.81	0.71	0.77	0.81	0.56	0.93	0.71	0.67	0.66	0.92	0.85
<i>AllVary</i>	0.90	0.88	0.96	0.85	0.80	0.37	0.82	0.68	0.77	0.67	0.84	0.68

^a GMD stations shown include Alert, Canada (ALT, 82° N, 62° W), Point Barrow, USA (BRW, 71° N, 156° W), Niwot Ridge, USA (NWR, 40° N, 105° W), Mauna Loa, Hawaii, USA (MLO, 20° N, 155° W), Ragged Point, Barbados (RPB, 13° N, 59° W), and South Pole, Antarctica (SPO, 90° S, 25° W). ^b “S” refers to the correlation slope (dy/dx) of the simulation–measurement comparison. ^c “R²” refers to the correlation coefficient.

**Figure 8.** Seasonal mean (2004) methane dry column (ppbv; left column) from the *Base* scenario and the relative difference (%; (*Base* observations)/observations; right column) with SCIAMACHY data. Simulated methane levels are gridded to the spatial resolution of the SCIAMACHY data.

sets (Ho et al., 2009; Deeter et al., 2012; Amnuaylojaroen et al., 2014). Based on direct comparison with NOAA ground-based “Tall Tower” measurements, Deeter et al. (2012) find that a smoothing error, which depends on the retrieval averaging kernels and CO variability in the lower troposphere, exhibits strong geographical and seasonal variability. Amnuaylojaroen et al. (2014) find that simulated CO concen-

trations are significantly and consistently higher than that of MOPITT V6 data over areas of biomass burning in Southeast Asia, similar to our results.

The primary advantage of the TES/MLS joint CO product is that it gives information on vertical distributions (Fig. 13). The simulation captures the tropospheric vertical profiles reasonably well (within $\pm 1\sigma$ of TES/MLS mean) at the se-

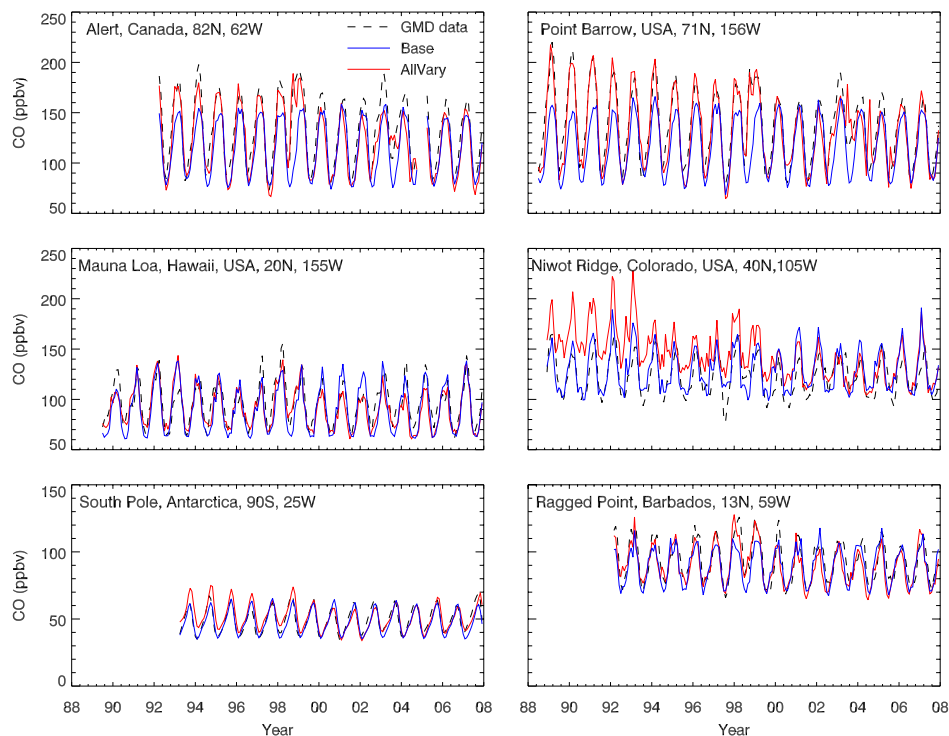


Figure 9. Monthly CO (ppbv) from the *Base* and *AllVary* scenarios and observations from six GMD stations. Similar plots for the other scenarios are given in Figs. S13 to S16.

lected locations in the Northern and Southern hemispheres and in all seasons, except over West Africa in boreal winter during the peak of biomass burning. The adjustment of the simulated CO with the TES/MLS averaging kernel (AK) significantly improves the agreement above 300 mb, over all locations and in all seasons, while near the surface the effect is geographically varying, in agreement with other studies (e.g., Deeter et al., 2012). Over the eastern US, the adjustment of simulated CO causes a slightly larger positive bias compared to that without adjustment. Though simulated CO is significantly improved near the surface, it is still biased high over West Africa by $\sim 50\%$ during the peak of biomass burning, also consistent with other studies (Amnuaylojaroen et al., 2014).

4 ECCOH as a tool for studying the nonlinear CH₄–CO–OH system

In this section, we (1) present the justification for simulating the nonlinear chemistry of the CH₄–CO–OH system as opposed to using a static climatology of OH distributions, and (2) demonstrate the utility of the ECCOH chemistry module for studying the CH₄–CO–OH system. In Sect. 4.1, we discuss the nontrivial, large-scale interannual variations of methane, CO, and OH in our scenarios. In Sect. 4.2, we discuss the considerable spatial and temporal heterogeneity of

OH and methane and CO loss rates, which would not be captured if a static climatology of OH distributions were used. In Sect. 4.3, we present the results of our sensitivity scenarios (Table 2), which demonstrate the utility of the ECCOH chemistry module for studying the CH₄–CO–OH system.

4.1 Large-scale interannual variations in methane, CO, and OH

Even on a global scale, there are large interannual variations in methane, CO, and OH. The deviations of mass-weighted concentrations of methane, CO, and OH for both the *Base* and *AllVary* scenarios are shown in Fig. 14. The magnitudes of the year-to-year deviations in methane are not substantially different between the two scenarios, since the *Base* scenario includes the important source of variation associated with anthropogenic methane emissions, and methane's background is large. On the other hand, the deviations for CO and OH are far greater in the *AllVary* scenario. The magnitude of the CO deviations is a factor of 10 greater in the *AllVary* scenario than the *Base* scenario, which has annually repeating CO emissions. The magnitude of the OH deviations increases ± 2 to $\pm 5\%$, though as discussed below, there are much larger variations on regional scales that are masked in the global average. In general, CO and OH deviations are coincident, but of opposite signs, as reaction of CO with OH is the primary sink for both gases on a global scale. Similar

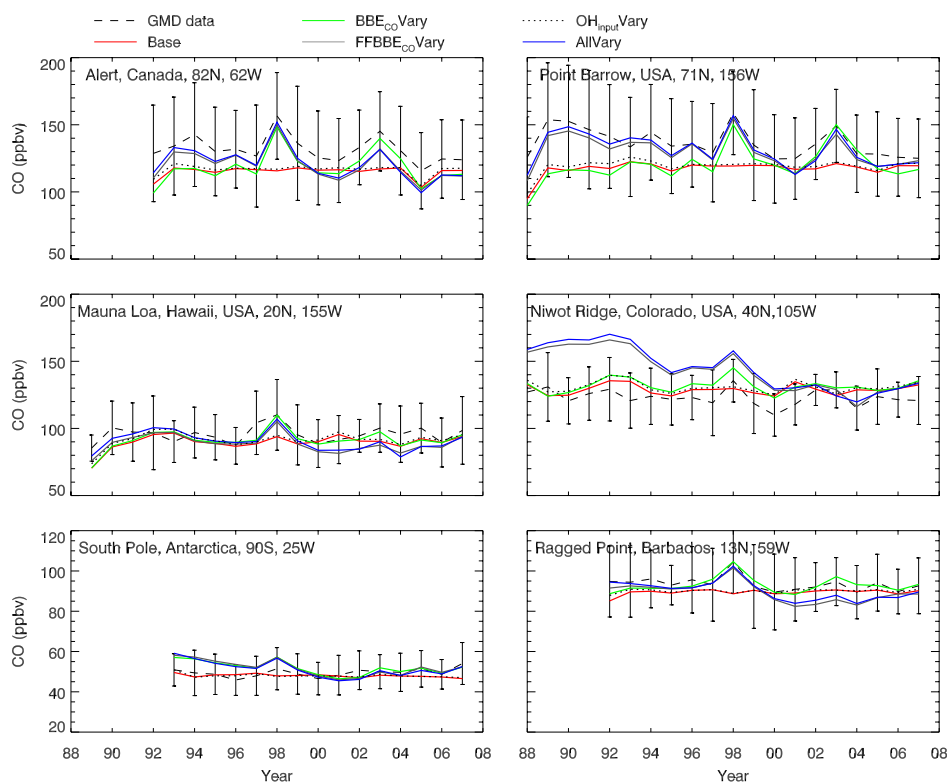


Figure 10. Annual mean CO (ppbv) from several scenarios and observations at six GMD stations. Vertical lines represent the standard deviation of the observed annual mean.

deviations are seen in the mid-latitudes of both hemispheres, indicating the global extent of some specific events, such as large biomass burning events. These results are also consistent with Voulgarakis et al. (2015), who, using full chemistry simulations, found large deviations ($> 15\%$) in CO using annually varying CO biomass burning emissions as compared to annually repeating emissions.

The nonlinear effects of the CH₄–CO–OH system on the temporal evolution of global mass-weighted methane are smaller, but significant, as compared to the effects of variations of methane emissions. The E_{CH_4} Vary scenario includes variations in anthropogenic and natural methane emissions and also variations in meteorology (e.g., temperature, water vapor) that influence the distributions of methane, CO, and OH. The AllVary scenario also includes variations in CO emissions and all the other factors that influence OH, such as the overhead ozone column, NO_x, tropospheric ozone, and VOCs. The influence of the nonlinear effects of the CH₄–CO–OH system is shown in the difference between the AllVary and E_{CH_4} Vary scenarios. For example, the shaded area between the two scenarios in Fig. 4 illustrates the combined effect of nonlinearities of the CH₄–CO–OH system on methane's growth rate. The growth rate in the AllVary scenario is about 4 ppb yr^{-1} higher than in the E_{CH_4} Vary scenario during the early 1990s, a time when stratospheric ozone

was impacted by the eruption of Mt. Pinatubo, emissions from the Soviet Union changed as it contracted economically, and there was a prolonged El Niño. While these factors caused changes in methane emissions, they also caused substantial variations in CO and OH (Duncan and Logan, 2008) that influenced methane's growth rate. Briefly in the mid-1990s, the growth rate in the AllVary scenario becomes lower than in the E_{CH_4} Vary scenario. The decline in methane growth rate in 1994–1997 is primarily related to the variability of the factors that influence OH (Fig. S4), while the other nonlinear feedbacks are primarily related to variability in CO emissions (Fig. S5). Worldwide, there were record wildfires in 1997 and 1998 that were associated with a record El Niño, which began in 1997, that transitioned to a record La Niña in 1998 (Duncan et al., 2003a, b). Consequently, there were large variations in CO (Duncan and Logan, 2008) that causes methane's growth rate to become higher again in the AllVary scenario. During the 2000s, a relatively quiet period with few large wildfires or notable ENSO events, the growth rate is lower in the AllVary scenario than the E_{CH_4} Vary scenario. In summary, the nonlinear effects of the CH₄–CO–OH system cause important fluctuations in methane's growth rate over our study period of $\pm 4 \text{ ppb yr}^{-1}$.

We compare simulated, mass-weighted pseudo first-order rate constants (k'), a proxy for OH interannual variations,

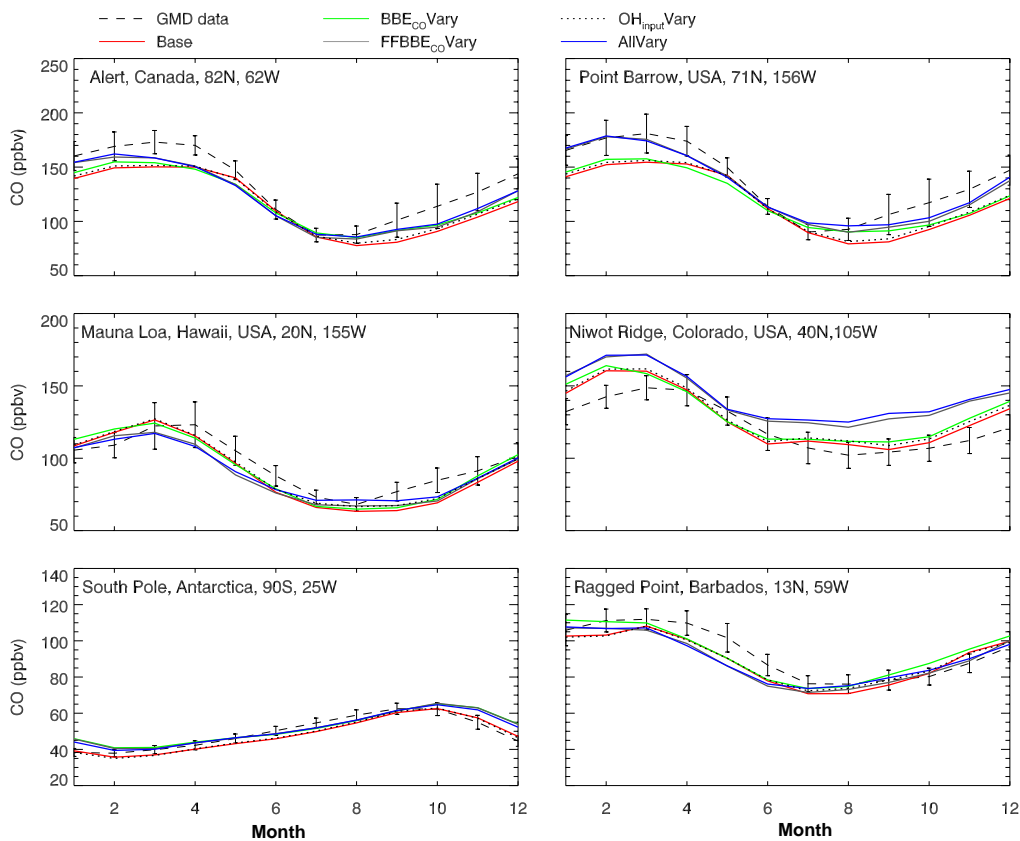


Figure 11. Monthly CO (ppbv) averaged over 1998–2007 for several scenarios and observations at six GMD stations. Vertical lines represent the standard deviation of the observed monthly mean.

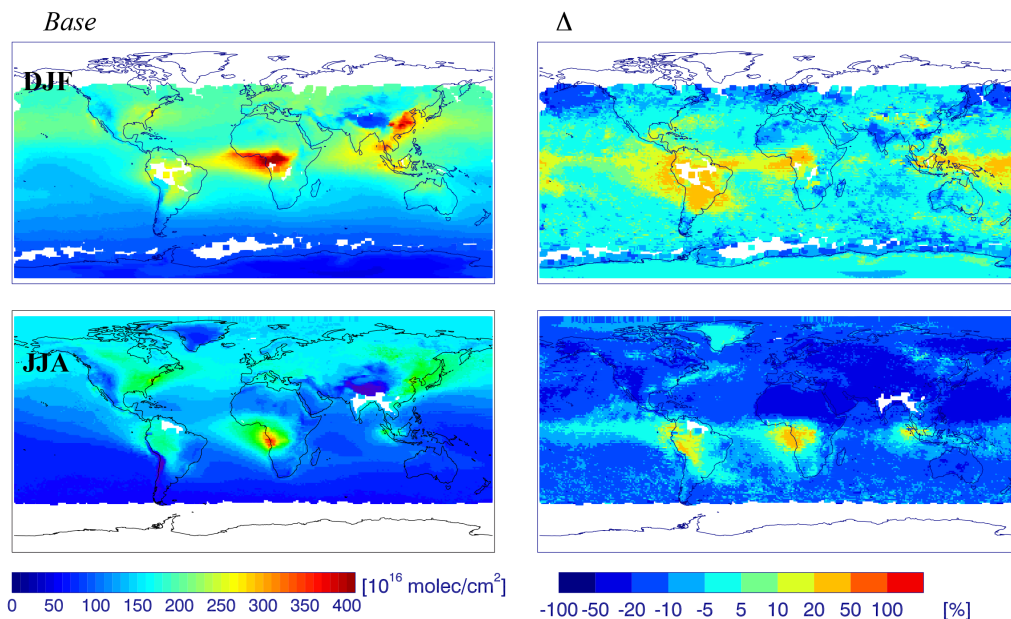


Figure 12. Seasonal mean (2006–2007) CO columns ($\times 10^{16}$ molecules cm^{-2}) from the *Base* scenario (left column) and the relative difference (%; (*Base* observations)/observations; right column) with MOPITT data.

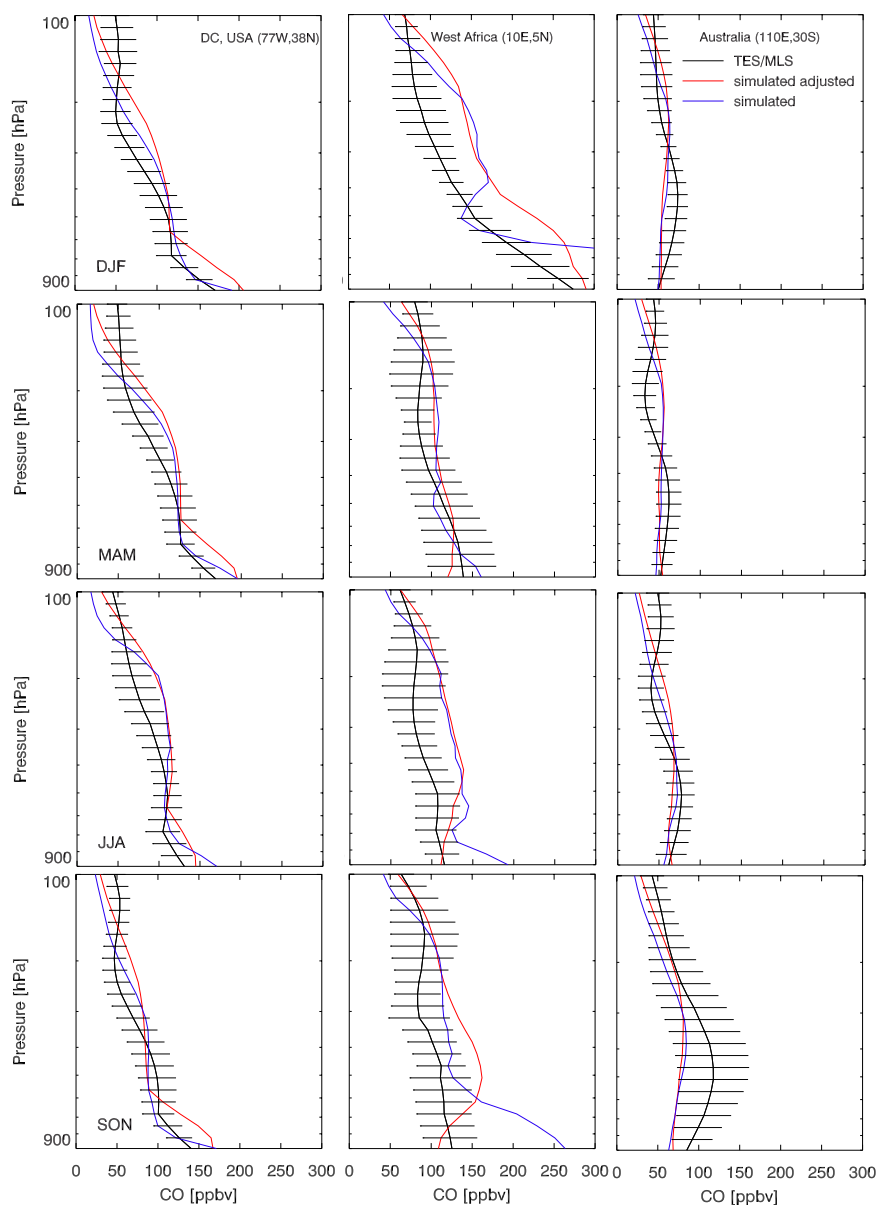


Figure 13. Seasonal mean (2006–2007) CO vertical profiles (ppbv) over select locations of TES/MLS data, the *Base* scenario (“simulated”), and the *Base* scenario adjusted with averaging kernels (“simulated adjusted”). The horizontal bars represent the standard deviation of the individual overpasses used to create the seasonal mean.

from each of our scenarios to that inferred from MCF measurements (Fig. 15; 1998–2007; Montzka et al., 2011). We find that none of our model scenarios is able to reproduce the inferred interannual OH variability of Montzka et al. (2011), though the simulated variability is of similar magnitude and within observational uncertainty. Our findings are consistent with other modeling studies (Montzka et al., 2011; Holmes et al., 2013; Murray et al., 2013, and references therein). While global interannual variations are informative, there can be considerable OH interannual variations regionally (as discussed in Sect. 4.2 and 4.3) that may not be reflected in

the global average (Lelieveld et al., 2002; Wild and Palmer, 2008).

Despite the lack of agreement between the inferred and simulated OH variations, this comparison exercise allows us to understand the contribution of various factors to the simulated interannual variations of tropospheric OH and, subsequently, the growth rate of methane (Fig. 4). As shown in Fig. 15, the *Base* scenario has $\pm 3\%$ interannual variability. This scenario includes interannual variations in meteorology, such as in clouds, water vapor, temperature, and solar radiation, which are known to be important drivers of OH

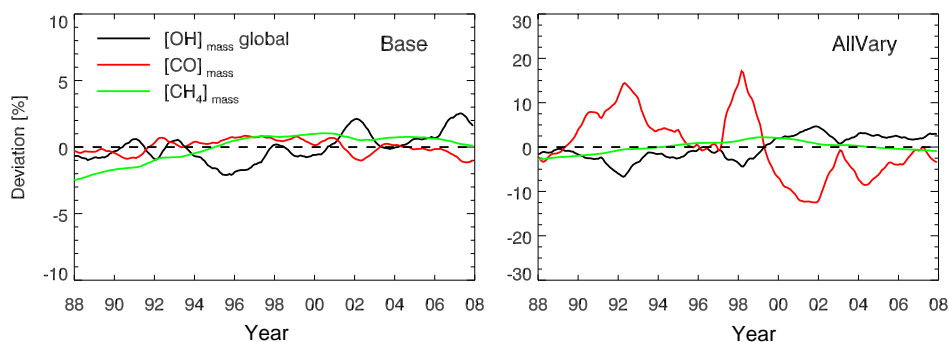


Figure 14. Deviations of tropospheric, mass-weighted OH, CO, and methane (12-month running mean) from the *Base* (left) and *AllVary* (right) scenarios. Note the different scales of the y axes.

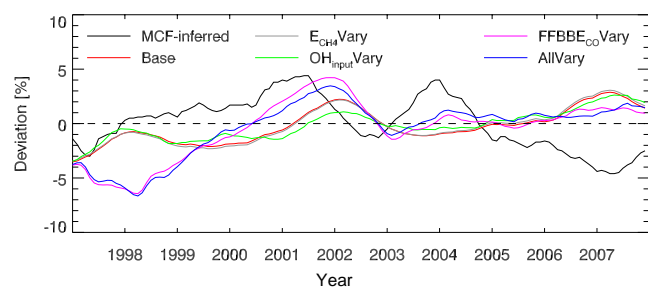


Figure 15. Deviations (%) of the global, mass-weighted, pseudo first-order rate constant (k') of the reaction of OH with MCF inferred from MCF measurements (black; adapted from Montzka et al., 2011) and from several scenarios.

(e.g., Rohrer and Berresheim, 2006; Rohrer et al., 2014). The only large deviation in OH from the *Base* scenario occurs in 1997 and 1998 in the *BBCO* *Vary* scenario. There were several major wildfires that account for this deviation, including fires in Indonesia, Mexico, and the boreal forests of Asia and North America (e.g., Duncan et al., 2003a). OH is lower in the *AllVary* scenario than the *Base* scenario because of higher CO emissions from the fires. For instance, Duncan et al. (2003b) used a model to show that the Indonesian wildfires in 1997 decreased OH levels by more than 20% over the Indian Ocean and by 5–10% over much of the tropics for several months. Lower OH during 1997 and 1998 in the *AllVary* scenario is consistent with the higher methane growth rate as compared to the *Base* scenario (Fig. 3).

ENSO affects the variability of sea surface temperatures, water vapor, deep convection, etc., and, subsequently, OH over large regions of the tropics. As shown in Fig. 16, the deviations of mass-weighted OH from various scenarios over Indonesia (100–150° E; 6° N–6° S) are generally anti-correlated with the Multivariate ENSO Index (MEI, Wolter et al., 2011), a proxy of ENSO. OH variations in the *Base* scenario, which includes meteorological variations that affect OH via variations in water vapor, clouds, etc., are $\pm 4\%$ ($R^2 = 0.20$), but much higher in the scenarios that include

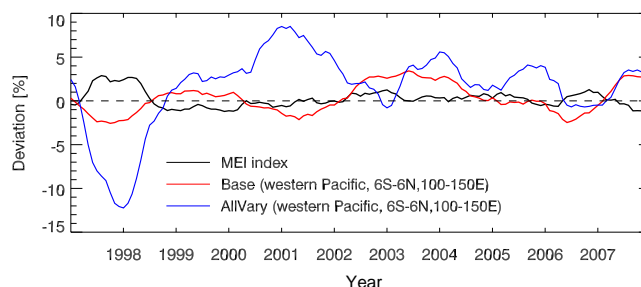


Figure 16. Deviation (%) of global, mass-weighted OH from various scenarios and the Multivariate ENSO Index (MEI). The lines are 12-month running means. Positive values of MEI indicate El Niño conditions and negative values indicate La Niña conditions. The correlation coefficient (R^2) for the *Base* scenario vs. the MEI index is 0.20, while for the *AllVary* scenario, it is 0.59.

variations in biomass burning emissions (e.g., the *AllVary* scenario), which better capture the ENSO variability ($R^2 = 0.59$).

4.2 Spatial and temporal distributions of the production/loss rates of Methane and CO

Any model simulation using annually repeating and archived OH will not accurately capture regional and interannual variations in the loss rates of methane and CO. A simulation using zonally averaged archived OH (e.g., Spivakovsky et al., 2000), such as was done in the TransCom MIP, will not capture any regional and interannual variations. For example, Figs. S7 and S12 reproduce Figs. 4a and 5, respectively, but include methane from a simulation using archived and annually repeating OH of the NASA Global Modeling Initiative (GMI) model (Duncan et al., 2007b; Strahan et al., 2007). The simulated longer methane lifetime (Fig. S7), using archived OH, leads to an accumulation of methane over the multi-decadal simulation. In this situation, the archived OH would need to be adjusted higher to improve the simulation of methane as compared to observations.

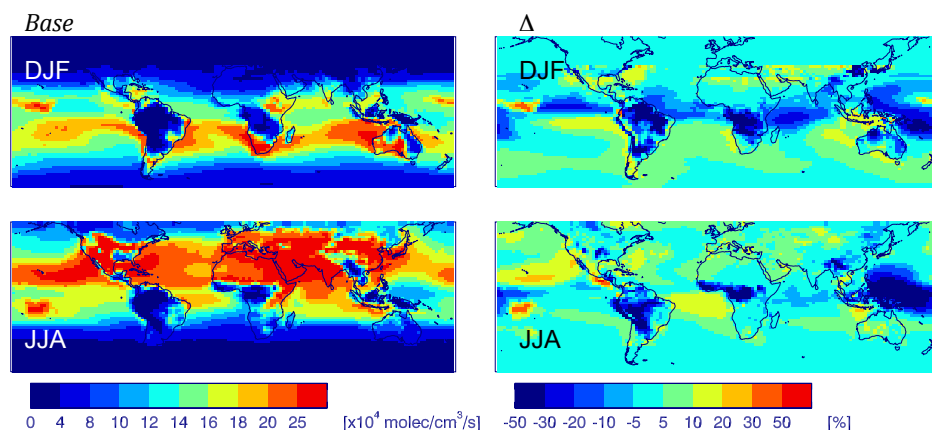


Figure 17. Seasonal mean (1988–2007) and mass-weighted tropospheric methane loss rate (left column; $\times 10^4$ molecules $\text{cm}^{-3} \text{s}^{-1}$) with the relative difference with the *AllVary* scenario ($(\text{Base} - \text{AllVary})/\text{Base}$; right column).

Even though methane is relatively well mixed in the troposphere due to its long lifetime, there is important spatial heterogeneity in methane's and CO's loss rates (Figs. 17 to 21), which is associated with the distribution of sources and reaction with OH, and changes in the density of air with altitude. The global methane loss rate maximizes during boreal summer and reaches a minimum during boreal winter (Fig. 17). Most methane loss occurs between 30°S and 30°N (Fig. 17) since OH is most abundant in this region and methane's reaction with OH is temperature dependent (Sander et al., 2011). In addition, most loss occurs near the surface despite higher OH in the mid-troposphere (Fig. 2) because of higher methane mole fractions near the surface (e.g., $\sim 3\%$ over Alaska but higher over source regions), the altitude dependence of air density, and the temperature dependence of the loss rate (Fig. 18). Methane's loss rates in the *AllVary* scenario are relatively higher, especially over biomass burning regions (Fig. 17), and have much higher spatial variability than in the *Base* scenario (Fig. 19). In contrast to methane, a higher proportion of CO is lost at Northern Hemisphere mid-latitudes as the CO loss rate is less temperature dependent than methane's and the lifetime is shorter (Fig. 20). The CO loss rate also varies strongly with altitude (not shown), similar to that of methane. The simulated seasonal mean loss rate of CO from the *AllVary* scenario is also relatively higher over biomass burning regions but lower over Asia (Fig. 20), and has a much higher variability that reaches up to $\sim 20\%$ compared to about 5% in the *Base* scenario (Fig. 21).

4.3 Factors that influence the nonlinear CH₄–CO–OH system

The differences in global abundances of CO and OH between our least complex (*Base*, Table 1) and most complex (*AllVary*, Table 2) scenarios are substantial and their impact on methane's evolution is nontrivial, as discussed in Sects. 4.1 and 4.2. Therefore, model studies of methane and/or CO,

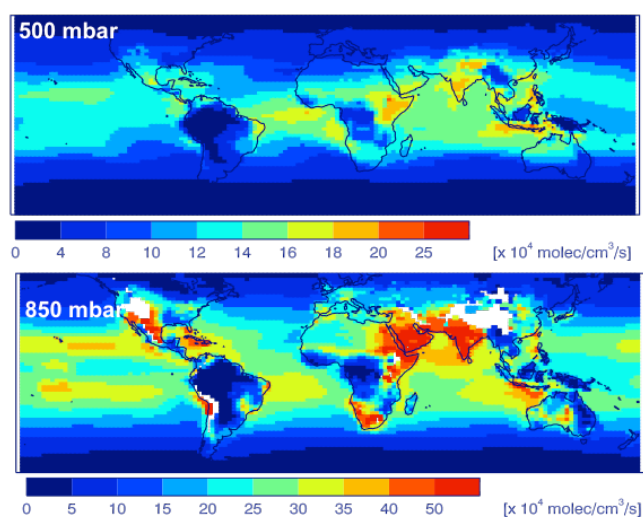


Figure 18. Mean methane loss rate (1988–2007; $\times 10^4$ molecules $\text{cm}^{-3} \text{s}^{-1}$) at 500 mb (top) and 850 mb (bottom) for the *Base* scenario.

which use archived fields of OH distributions, will not capture these important nonlinear feedbacks of the CH₄–CO–OH system (e.g., Fig. 4). Here, we discuss the contribution of various factors to the observed spatial distributions and temporal evolution of observed methane, CO, and OH to demonstrate the utility of the ECCOH chemistry module for studying the CH₄–CO–OH system. We provide a brief summary of our conclusions from the scenarios at the end of this section.

E_{CH₄} Vary scenario. In the *E_{CH₄} Vary* scenario, all methane emissions are annually varying (Fig. S1). Variations in emissions from wetlands are the largest single contributor to global interannual variations, with biomass burning being a lesser contributor (e.g., Bousquet et al., 2006). Patra et al. (2011) reported that up to 60% of methane's observed interannual variation can be explained by variations in me-

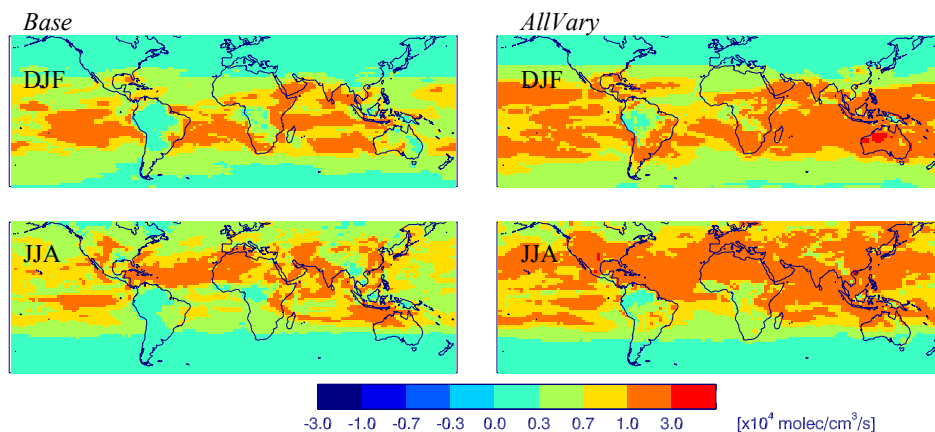


Figure 19. Seasonal mean (1988–2007) standard deviation of tropospheric methane loss rates ($\times 10^4$ molecules $\text{cm}^{-3} \text{s}^{-1}$) from the *Base* (left column) and *AllVary* (right column) scenarios.

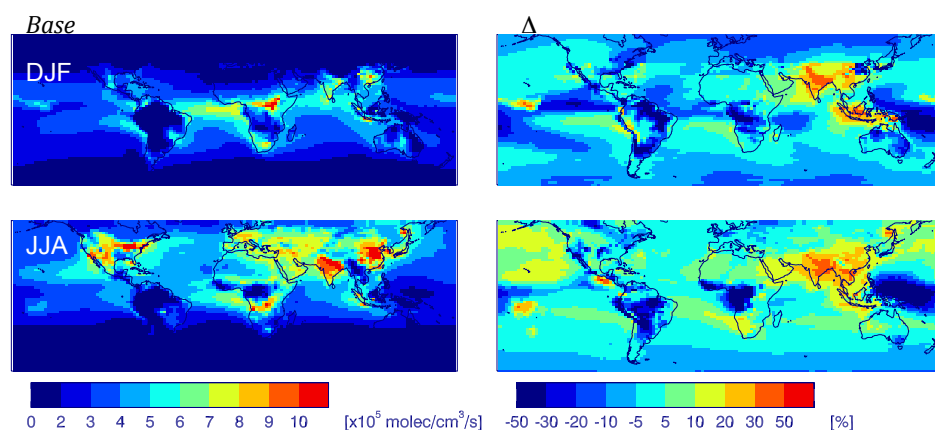


Figure 20. Seasonal mean (1988–2007), mass-weighted tropospheric CO loss rates (left column; $\times 10^5$ molecules $\text{cm}^{-3} \text{s}^{-1}$) from the *Base* scenario, and relative difference (%) between the *Base* and *AllVary* scenarios ($(\text{Base} - \text{AllVary}) / \text{Base}$; right column).

teology as well as interannual variations in wetland and biomass burning emissions. Given the high methane background concentration, the spatial differences of methane columns between the E_{CH_4} *Vary* and *Base* scenarios are rather small (about ± 5 ppb (-1 to 1%)) over most of the globe when taken as seasonal averages of 1988–2007 (Fig. S19). Consistent with the annually varying natural emissions of methane, the largest differences occur over rice-producing regions of India and Bangladesh (up to $\sim 5\%$) and the wetlands of South America (down to -5%), including the Pantanal. The simulated methane monthly variations from the E_{CH_4} *Vary* scenario are in better agreement for the Northern Hemisphere high-latitude GMD station observations as compared to the *Base* scenario (Fig. S8), which is also consistent with the findings of the TransCom MIP (Patra et al., 2011). The impact of annually varying natural methane emissions has a small effect (-1 to 1%), as expected, on the spatial

distributions of CO and OH because of the slow reaction rate of methane with OH (Fig. S19, Table 4).

BBE_{CO} *Vary* and $FFBBE_{\text{CO}}$ *Vary* scenarios. We developed these scenarios to understand the influence of annually varying CO emissions from biomass burning and fossil fuel combustion (Fig. S2) on the observed interannual variation of methane, CO, and OH. Including annually varying biomass burning emissions (BBE_{CO} *Vary*) improves the mean agreement of the simulated CO with GMD observations (mean $S = 0.83$, $R^2 = 0.70$, Table 4), but not at all individual GMD stations (Table 4). Improvements occur particularly during the years with large fires (e.g., 1997, 1998, 2003, 2004; Figs. 9 to 11). Adding annually varying anthropogenic CO emissions in addition to annually varying biomass burning emissions ($FFBBE_{\text{CO}}$ *Vary*) further improves the mean comparison (mean $S = 0.88$), particularly in the Northern Hemisphere during the 1990s (Fig. 10). Overall, annually varying CO emissions ($FFBBE_{\text{CO}}$ *Vary*) have a significant im-

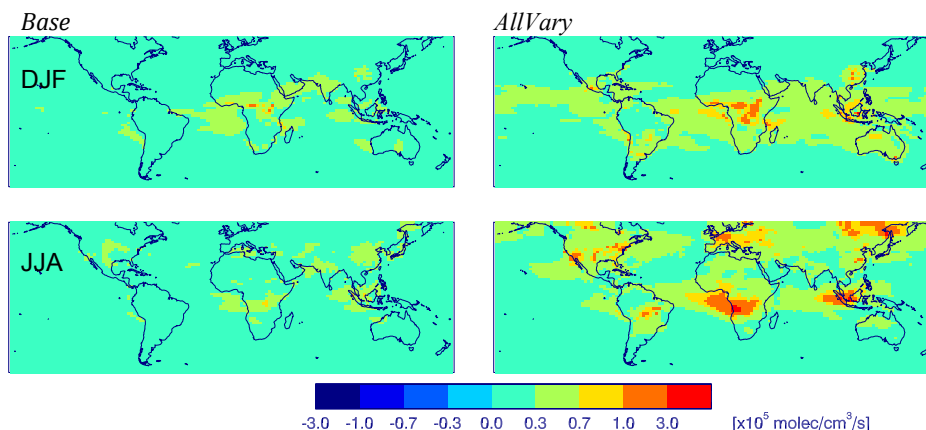


Figure 21. Seasonal mean (1988–2007) standard deviation of tropospheric CO loss rates ($\times 10^5$ molecules $\text{cm}^{-3} \text{s}^{-1}$) from the *Base* (left column) and *AllVary* (right column) scenarios.

impact on the spatial distributions of tropospheric CO ($\pm 20\%$) and OH ($\pm 10\%$) relative to the *Base* scenario, and influence methane by $\pm 1\%$ (Fig. S21, Table 4). Simulating annually varying CO biomass burning emissions (i.e., the *BBCO Vary* scenario) improves simulated methane relative to the *Base* scenario as compared to observations (mean $S = 0.97$, $R^2 = 0.76$, Table 4).

OH_{input} Vary scenario. In this scenario, we look at the impact of other causal factors that influence OH, including trends in NO_x and VOC emissions and the overhead ozone column (Table 2). For example, both variations in the overhead ozone column and NO emissions from lightning are known to cause variations in global OH (e.g., Duncan and Logan, 2008; Murray et al., 2013). Together, these causal factors have a significant influence on the spatial distributions of OH ($\pm 20\%$) and CO ($\pm 5\%$) relative to the *Base* scenario and a $\pm 1\%$ effect on methane (Figs. S4, S20, Table 4).

AllVary scenario. In this scenario, we investigate the combined effect of all variables (Table 2) on the simulated distributions of methane, CO, and OH. The seasonal mean spatial (not shown) and zonal (Fig. 2) distributions of OH are quite comparable to that of the *Base* scenario. The interannual variations in the seasonal mean OH (Fig. 22) are significantly higher ($\sim 20\%$) as compared to the *Base* scenario ($< 5\%$, Sect. 3.1), which is related to the annually varying methane and CO emissions as well as OH constraints in this scenario. There are large differences in the spatial distributions of methane ($\pm 5\%$), CO ($\pm 20\%$), and OH ($\pm 20\%$) between the *Base* and *AllVary* scenarios (Fig. S22, Table 4). Despite large spatial differences in OH, the global, mean MCF lifetime for the *AllVary* scenario, which ranges from 6.01 (± 0.51) to 6.67 (± 0.61) years over the simulation period, is not significantly different from that of the *Base* scenario.

Summary of key findings of sensitivity studies. Overall, variations in anthropogenic and natural methane emissions drive the majority of global variations in observed methane,

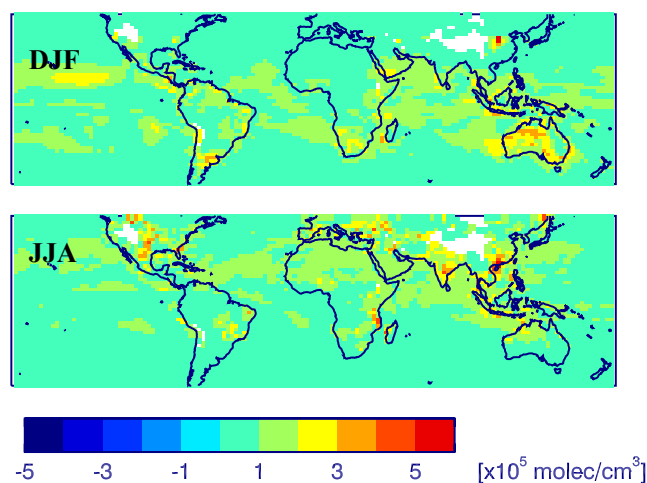


Figure 22. Seasonal mean (1988–2007) standard deviations of OH ($\times 10^5$ molecules cm^{-3}) at 850 mbar for the *AllVary* scenario.

and variations in anthropogenic and natural CO emissions drive the majority of global variations in observed CO. These results are consistent with the findings of other literature studies (e.g., Duncan and Logan, 2008; Patra et al., 2011). We find that the influence of variations of CO emissions and factors that influence OH (e.g., overhead ozone column, VOCs, NO_x) have a significant net effect on the distributions and temporal evolution of methane, CO, and OH. This result is consistent with the findings of Duncan and Logan (2008) for CO and OH. The significant influence of the combined nonlinear feedbacks on methane is shown in the difference between the *AllVary* and *E_{CH₄} Vary* scenarios (e.g., Fig. 4).

Accurate quantification of the magnitude of the combined nonlinear feedbacks is ultimately dependent on the uncertainties and errors of emissions, such as those discussed in Sect. 3, and independent variables, all of which have their

own uncertainties, used in the parameterization of OH. With our sensitivity simulations, we discussed instances when changes to emissions and/or the input to the parameterization of OH improved or worsened the simulated methane and CO. In some instances, simulated methane and/or CO from the least complex *Base* scenario more favorably agreed with observations than the other more complex scenarios, including methane in the most complex *AllVary* scenario (e.g., Table 4, Fig. 4). However, in these instances, better correlation does not necessarily imply that a simpler scenario, such as the *Base* scenario or a scenario that uses archived and annually repeating OH, is inherently better. The best scenario is one that accurately simulates the complex interactions of the factors that influence the CH₄–CO–OH system, which will give confidence in the response of the system to perturbations, such as from large interannual variations in wetland fluxes, biomass burning, ENSO, and volcanic eruptions. The next steps for our research include quantifying the (1) sensitivity of the simulated CH₄–CO–OH system to uncertainties in the factors (e.g., water vapor, clouds, trace gases) that control tropospheric OH so as to improve simulated methane and CO with observations, and (2) the influence of potential large atmospheric carbon perturbations in a warming world, such as may occur from permafrost thaw, methane hydrate release, and enhanced biomass burning.

5 Summary

We present the fully interactive, computationally Efficient CH₄–CO–OH (ECCOH) chemistry module, which we implemented in the NASA GEOS-5 AGCM. To demonstrate the utility of the ECCOH chemistry module, we exercised the module with a set of scenarios to simulate the influence of various causal factors on OH and the observed variations in methane and CO over 1988–2007, which gives confidence in the fidelity of the module for scientific research. Discrepancies between the output and observations are largely explained by known deficiencies (as reported in the literature) in the methane and CO emissions used as input to the ECCOH chemistry module and AGCM. Through our simulations, we show the importance of using an interactive CH₄–CO–OH system as opposed to using static, archived OH fields, as nonlinear feedbacks on methane, CO, and OH are non-trivial. For example, nonlinear feedbacks modulate the global methane growth rate over our study period (± 20 ppbv yr⁻¹) by ± 4 ppbv yr⁻¹ (Fig. 4).

Code availability

The GEOS-5 source code is available under the NASA Open Source Agreement at <http://opensource.gsfc.nasa.gov/projects/GEOS-5/>.

The GEOS-5 CCM version that includes our ECCOH chemistry module is available in the supple-

mentary material. For documentation and installation instructions, please visit the GEOS-5 online wiki: http://geos5.org/wiki/index.php?title=GEOS-5_Earth_System_Modeling_and_Data_Assimilation.

The Supplement related to this article is available online at doi:10.5194/gmd-9-799-2016-supplement.

Acknowledgements. This work was supported by the NASA Modeling, Analysis and Prediction and Interdisciplinary Science programs. We would like to thank the SCIAMACHY WFM-DOAS team at the University of Bremen IUP/IFE for using their methane L3 product as well as the TES/MLS Aura team for using their L2 CO product, and Stephen Montzka (NOAA) for providing MCF-inferred OH deviations for comparison. MOPITT CO column data were obtained from the NASA Langley Research Center Atmospheric Science Data Center. We would also like to thank Stacey Frith for providing the output of the GEOS-5 CCM full chemistry simulations. Earlier model development of the ECCOH chemistry module by Elena Yegorova is appreciated. Useful discussions with Prabir Patra (RIGC/JAMSTEC), Huisheng Bian, Junhua Liu, and Jerald Ziemke (NASA GSFC), as well as technical support from Michael Manyin, Yasuko Yoshida, and Eric Nielsen (NASA GSFC), are gratefully acknowledged.

Edited by: P. Jöckel

References

- Amnuaylojaroen, T., Barth, M. C., Emmons, L. K., Carmichael, G. R., Kreasuwun, J., Prasadwattanaseree, S., and Chantara, S.: Effect of different emission inventories on modeled ozone and carbon monoxide in Southeast Asia, *Atmos. Chem. Phys.*, 14, 12983–13012, doi:10.5194/acp-14-12983-2014, 2014.
- Bousquet, P., Ciais, P., Miller, J. B., Dlugokencky, E. J., Hauglustaine, D. A., Prigent, C., Van der Werf, G. R., Peylin, P., Brunke, E. G., Carouge, C., Langenfelds, R. L., Lathiere, J., Papa, F., Ramonet, M., Schmidt, M., Steele, L. P., Tyler, S. C., and White, J.: Contribution of anthropogenic and natural sources to atmospheric methane variability, *Nature*, 443, 439–443, 2006.
- Bovensmann, H., Burrows, J. P., Buchwitz, M., Frerick, J., Noël, S., Rozanov, V. V., Chance, K. V., and Goede, A.: SCIAMACHY – Mission Objectives and measurement Modes, *J. Atmos. Sci.*, 56, 127–150, 1999.
- Chameides, W., Liu, S. C., and Cicerone, R. J.: Possible variations in atmospheric methane, *J. Geophys. Res.*, 81, 4997–5001, 1976.
- Chen, Y.-H. and Prinn, R. G.: Estimation of atmospheric methane emissions between 1996 and 2001 using a three-dimensional global chemical transport model, *J. Geophys. Res.*, 111, D10307, doi:10.1029/2005JD006058, 2006.
- Deeter, M. N.: MOPITT (Measurement of Pollution in the Troposphere) Version6 Product User's Guide, available at: http://www2.acd.ucar.edu/sites/default/files/mopitt/v6_users_guide_201309.pdf (last access: 28 May 2015), 2013.

- Deeter, M. N., Worden, H. M., Edwards, D. P., Gille, J. C., and Andrews, A. E.: Evaluation of MOPITT retrievals of lower tropospheric carbon monoxide over the United States, *J. Geophys. Res.*, 117, D13306, doi:10.1029/2012JD017553, 2012.
- Dlugokencky, E. J., Lang, P. M., and Masarie, K. A.: Atmospheric Methane Dry Air Mole Fractions from the NOAA ESRL Carbon Cycle Cooperative Global Air Sampling Network, 1983–2014, Version: 2015-08-03, available at: ftp://aftp.cmdl.noaa.gov/data/trace_gases/ch4/flask/surface, last access: 22 February 2016.
- Dlugokencky, E. J., Lang, P. M., Crotwell, A. M., Masarie, K. A., and Crotwell, M. J.: Atmospheric Methane Dry Air Mole Fractions from the NOAA ESRL Carbon Cycle, Cooperative Global Air Sampling Network, 1983–2013, Version: 2014-06-24, 2014.
- Duncan, B. N. and Logan, J. A.: Model analysis of the factors regulating the trends and variability of carbon monoxide between 1988 and 1997, *Atmos. Chem. Phys.*, 8, 7389–7403, doi:10.5194/acp-8-7389-2008, 2008.
- Duncan, B. N., Portman, D., Bey, I., and Spivakovsky, C. M.: Parameterization of OH for efficient computation in chemical tracer models, *J. Geophys. Res.*, 105, 12259–12262, 2000.
- Duncan, B. N., Martin, R. V., Staudt, A. C., Yevich, R. M., and Logan, J. A.: Interannual and Seasonal Variability of Biomass Burning Emissions Constrained by Satellite Observations, *J. Geophys. Res.*, 108, 4040, doi:10.1029/2002JD002378, 2003a.
- Duncan, B. N., Bey, I., Chin, M., Mickley, L. J., Fairlie, T. D., Martin, R. V., and Matsueda, H.: Indonesian Wildfires of 1997: Impact on Tropospheric Chemistry, *J. Geophys. Res.*, 108, 4458, doi:10.1029/2002JD003195, 2003b.
- Duncan, B. N., Logan, J. A., Bey, I., Megretskaya, I. A., Yantosca, R. M., Novelli, P. C., Jones, N. B., and Rinsland, C. P.: Global budget of CO, 1988–1997: Source estimates and validation with a global model, *J. Geophys. Res.*, 112, D22301, doi:10.1029/2007JD008459, 2007a.
- Duncan, B. N., Strahan, S. E., Yoshida, Y., Steenrod, S. D., and Livesey, N.: Model study of the cross-tropopause transport of biomass burning pollution, *Atmos. Chem. Phys.*, 7, 3713–3736, doi:10.5194/acp-7-3713-2007, 2007b.
- Elshorbany, Y. F., Barnes, I., Becker, K. H., Kleffmann, J., and Wiesen, P.: Sources and Cycling of Tropospheric Hydroxyl Radicals – An Overview, *Z. Phys. Chem.*, 224, 967–987, doi:10.1524/zpch.2010.6136, 2010.
- Elshorbany, Y. F., Kleffmann, J., Hofzumahaus, A., Kurtenbach, R., Wiesen, P., Dorn, H.-P., Schlosser, E., Brauers, T., Fuchs, H., Rohrer, F., Wahner, A., Kanaya, Y., Yoshino, A., Nishida, S., Kajii, Y., Martinez, M., Rudolf, M., Harder, H., Lelieveld, J., Elste, T., Plass-Dülmer, C., Stange, G., and Berresheim, H.: HO_x Budgets during HO_xComp: a Case Study of HO_x Chemistry under NO_x limited Conditions, *J. Geophys. Res.*, 117, D03307, doi:10.1029/2011JD017008, 2012a.
- Elshorbany, Y. F., Steil, B., Brühl, C., and Lelieveld, J.: Impact of HONO on global atmospheric chemistry calculated with an empirical parameterization in the EMAC model, *Atmos. Chem. Phys.*, 12, 9977–10000, doi:10.5194/acp-12-9977-2012, 2012b.
- Elshorbany, Y. F., Crutzen, P. J., Steil, B., Pozzer, A., Tost, H., and Lelieveld, J.: Global and regional impacts of HONO on the chemical composition of clouds and aerosols, *Atmos. Chem. Phys.*, 14, 1167–1184, doi:10.5194/acp-14-1167-2014, 2014.
- Fiore, A. M., Jacob, D. J., Field, B. D., Streets, D. G., Fernandes, S. D., and Jang, C.: Linking air pollution and climate change: The case for controlling methane, *Geophys. Res. Lett.*, 29, 1919, doi:10.1029/2002GL015601, 2002.
- Fiore, A. M., Horowitz, L. W., Dlugokencky, E. J., and West, J. J.: Impact of meteorology and emissions on methane trends, 1990–2004, *Geophys. Res. Lett.*, 33, L12809, doi:10.1029/2006GL026199, 2006.
- Fiore, A. M., Dentener, F. J., Wild, O., Cuvelier, C., Schultz, M. G., Hess, P., Textor, C., Schulz, M., Doherty, R. M., Horowitz, L. W., MacKenzie, I. A., Sanderson, M. G., Shindell, D. T., Stevenson, D. S., Szopa, S., Van Dingenen, R., Zeng, G., Ather-ton, C., Bergmann, D., Bey, I., Carmichael, G., Collins, W. J., Duncan, B. N., Faluvegi, G., Folberth, G., Gauss, M., Gong, S., Hauglustaine, D., Holloway, T., Isaksen, I. S. A., Jacob, D. J., Jonson, J. E., Kaminski, J. W., Keating, T. J., Lupu, A., Marmor, E., Montanaro, V., Park, R. J., Pitari, G., Pringle, K. J., Pyle, J. A., Schroeder, S., Vivanco, M. G., Wind, P., Wojcik, G., Wu, S., and Zuber, A.: Multimodel estimates of intercontinental source-receptor relationships for ozone pollution, *J. Geophys. Res.*, 114, D04301, doi:10.1029/2008JD010816, 2009.
- Frankenberg, C., Aben, I., Bergamaschi, P., Dlugokencky, E. J., van Hees, R., Houweling, S., van der Meer, P., Snel, R., and Tol, P.: Global column-averaged methane mixing ratios from 2003 to 2009 as derived from SCIAMACHY: Trends and variability, *J. of Geophys. Res.*, 116, D04302, doi:10.1029/2010JD014849, 2011.
- Fuchs, H., Hofzumahaus, A., Rohrer, F., Bohn, B., Brauers, T., Dorn, H.-P., Hasseler, R., Holland, F., Kaminski, M., Li, X., Lu, K., Nehr, S., Tillmann, R., Wegener, R., and Wahner, A.: Experimental evidence for efficient hydroxyl radical regeneration in isoprene oxidation, *Nat. Geosci.* 6, 1023–1026, doi:10.1038/ngeo1964, 2013.
- Fujino, J., Nair, R., Kainuma, M., Masui, T., and Matsuoka, Y.: Multigas mitigation analysis on stabilization scenarios using aim global model, *Energy J.*, Special issue, 3, 343–354, 2006.
- Giglio, L., Randerson, J. T., van der Werf, G. R., Kasibhatla, P. S., Collatz, G. J., Morton, D. C., and DeFries, R. S.: Assessing variability and long-term trends in burned area by merging multiple satellite fire products, *Biogeosciences*, 7, 1171–1186, doi:10.5194/bg-7-1171-2010, 2010.
- Gludemans, A. M. S., Schrijver, H., Hasekamp, O. P., and Aben, I.: Error analysis for CO and CH₄ total column retrievals from SCIAMACHY 2.3 μm spectra, *Atmos. Chem. Phys.*, 8, 3999–4017, doi:10.5194/acp-8-3999-2008, 2008.
- Hijioka, Y., Matsuoka, Y., Nishimoto, H., Masui, T., and Kainuma, M.: Global GHG emission scenarios under GHG concentration stabilization targets, *J. Glob. Environ. Eng.*, 13, 97–108, 2008.
- Ho, S.-P., Edwards, D. P., Gille, J. C., Luo, M., Osterman, G. B., Kulawik, S. S., and Worden, H.: A global comparison of carbon monoxide profiles and column amounts from Tropospheric Emission Spectrometer (TES) and Measurements of Pollution in the Troposphere (MOPITT), *J. Geophys. Res.*, 114, D21307, doi:10.1029/2009JD012242, 2009.
- Holmes, C. D., Prather, M. J., Søvdø, O. A., and Myhre, G.: Future methane, hydroxyl, and their uncertainties: key climate and emission parameters for future predictions, *Atmos. Chem. Phys.*, 13, 285–302, doi:10.5194/acp-13-285-2013, 2013.
- Houweling, S., Krol, M., Bergamaschi, P., Frankenberg, C., Dlugokencky, E. J., Morino, I., Notholt, J., Sherlock, V., Wunch, D., Beck, V., Gerbig, C., Chen, H., Kort, E. A., Röckmann, T., and

- Aben, I.: A multi-year methane inversion using SCIAMACHY, accounting for systematic errors using TCCON measurements, *Atmos. Chem. Phys.*, 14, 3991–4012, doi:10.5194/acp-14-3991-2014, 2014.
- Kirschke, S., Bousquet, P., Ciais, P., Saunoy, M., Canadell, J. G., Dlugokencky, E. J., Bergamaschi, P., Bergmann, D., Blake, D. R., Bruhwiler, L., Cameron-Smith, P., Castaldi, S., Chevallier, F., Feng, L., Fraser, A., Heimann, M., Hodson, E. L., Houweling, S., Josse, B., Fraser, P. J., Krummel, P. B., Lamarque, J.-F., Langenfelds, R. L., Le Quééré, C., Naik, V., O'Doherty, S., 15 Palmer, P. I., Pison, I., Plummer, D., Poulter, B., Prinn, R. G., Rigby, M., Ringeval, B., Santini, M., Schmidt, M., Shindell, D. T., Simpson, I. J., Spahni, R., Steele, L. P., Strode, S. A., Sudo, K., Szopa, S., van der Werf, G. R., Voulgarakis, A., van Weele, M., Weiss, R. F., Williams, J. E., and Zeng, G.: Three decades of global methane sources and sinks, *Nat. Geosci.*, 6, 813–823, doi:10.1038/ngeo1955, 2013.
- Lamarque, J.-F., Shindell, D. T., Josse, B., Young, P. J., Cionni, I., Eyring, V., Bergmann, D., Cameron-Smith, P., Collins, W. J., Doherty, R., Dalsoren, S., Faluvegi, G., Folberth, G., Ghan, S. J., Horowitz, L. W., Lee, Y. H., MacKenzie, I. A., Nagashima, T., Naik, V., Plummer, D., Righi, M., Rumbold, S. T., Schulz, M., Skeie, R. B., Stevenson, D. S., Strode, S., Sudo, K., Szopa, S., Voulgarakis, A., and Zeng, G.: The Atmospheric Chemistry and Climate Model Intercomparison Project (ACCMIP): overview and description of models, simulations and climate diagnostics, *Geosci. Model Dev.*, 6, 179–206, doi:10.5194/gmd-6-179-2013, 2013.
- Lawrence, M. G., Jöckel, P., and von Kuhlmann, R.: What does the global mean OH concentration tell us?, *Atmos. Chem. Phys.*, 1, 37–49, doi:10.5194/acp-1-37-2001, 2001.
- Lelieveld, J., Peters, W., Dentener, F. J., and Krol, M. C.: Stability of tropospheric hydroxyl chemistry, *J. Geophys. Res.*, 107, 4715, doi:10.1029/2002JD002272, 2002.
- Lin, S.-J.: A “vertically Lagrangian” finite-volume dynamical core for global models, *Mon. Weather Rev.*, 132, 2293–2307, 2004.
- Luo, M., Read, W., Kulawik, S., Worden, J., Livesey, N., Bowman, K., and Herman, R.: Carbon monoxide (CO) vertical profiles derived from joined TES and MLS measurements, *J. Geophys. Res. Atmos.*, 118, 10601–10613, doi:10.1002/jgrd.50800, 2013.
- Molod, A., Takacs, L., Suarez, M., Bacmeister, J., Song, I.-S., and Eichmann, A.: The GEOS-5 Atmospheric General Circulation Model: Mean Climate and Development from MERRA to Fortuna, NASA/TM-2012-104606, Technical Report Series on Global Modeling and Data Assimilation, edited by: Suarez, M., Vol. 28, available at: <http://gmao.gsfc.nasa.gov/pubs/docs/tm28.pdf> (last access: 27 October 2015), 2012.
- Monks, S. A., Arnold, S. R., Emmons, L. K., Law, K. S., Turquety, S., Duncan, B. N., Flemming, J., Huijnen, V., Tilmes, S., Langner, J., Mao, J., Long, Y., Thomas, J. L., Steenrod, S. D., Raut, J. C., Wilson, C., Chipperfield, M. P., Diskin, G. S., Weinheimer, A., Schlager, H., and Ancellet, G.: Multi-model study of chemical and physical controls on transport of anthropogenic and biomass burning pollution to the Arctic, *Atmos. Chem. Phys.*, 15, 3575–3603, doi:10.5194/acp-15-3575-2015, 2015.
- Montzka, S. A., Krol, M., Dlugokencky, E., Hall, B., Joeckel, P., and Lelieveld, J.: Small interannual variability of global atmospheric hydroxyl, *Science*, 331, 67–69, doi:10.1126/science.1197640, 2011.
- Murray, L. T., Logan, J. A., and Jacob, D. J.: Interannual variability in tropical tropospheric ozone and OH: The role of lightning, *J. Geophys. Res. Atmos.*, 118, 11468–11480, doi:10.1002/jgrd.50857, 2013.
- Myhre, G., Shindell, D., Breion, F.-M., Collins, W., Fuglestedt, J., Huang, J., Koch, D., Lamarque, J.-F., Lee, D., Mendoza, B., Nakajima, T., Robock, A., Stephens, G., Takemura, T., and Zhang, H.: Anthropogenic and natural radiative forcing, in: *Climate Change 2013: The Physical Science Basis. Contribution of Working Group I to the Fifth Assessment Report of the Intergovernmental Panel on Climate Change*, edited by: Stocker, T. F., Qin, D., Plattner, G.-K., Tignor, M., Allen, S. K., Boschung, J., Nauels, A., Xia, Y., Bex, V., and Midgley, P. M., available at: http://www.climatechange2013.org/images/report/WG1AR5_ALL_FINAL.pdf (last access: 27 October 2015), 2013.
- Naik, V., Voulgarakis, A., Fiore, A. M., Horowitz, L. W., Lamarque, J.-F., Lin, M., Prather, M. J., Young, P. J., Bergmann, D., Cameron-Smith, P. J., Cionni, I., Collins, W. J., Dalsøren, S. B., Doherty, R., Eyring, V., Faluvegi, G., Folberth, G. A., Josse, B., Lee, Y. H., MacKenzie, I. A., Nagashima, T., van Noije, T. P. C., Plummer, D. A., Righi, M., Rumbold, S. T., Skeie, R., Shindell, D. T., Stevenson, D. S., Strode, S., Sudo, K., Szopa, S., and Zeng, G.: Preindustrial to present-day changes in tropospheric hydroxyl radical and methane lifetime from the Atmospheric Chemistry and Climate Model Intercomparison Project (ACCMIP), *Atmos. Chem. Phys.*, 13, 5277–5298, doi:10.5194/acp-13-5277-2013, 2013.
- Novelli, P., Steele, P., and Tans, P. P.: Mixing ratios of carbon monoxide in the troposphere, *J. Geophys. Res.*, 102, 12855–12861, doi:10.1029/92JD02010, 1992.
- Novelli, P., Masarie, K. A., and Lang, P. M.: Distributions and recent changes in carbon monoxide in the lower troposphere, *J. Geophys. Res.*, 103, 19015–19033, 1998.
- Oman, L. D., Ziemke, J. R., Douglass, A. R., Waugh, D. W., Lang, C., Rodriguez, J. M., and Nielsen, J. E.: The response of tropical tropospheric ozone to ENSO, *Geophys. Res. Lett.*, 38, L13706, doi:10.1029/2011GL047865, 2011.
- Ott, L., Duncan, B., Pawson, S., Colarco, P., Chin, M., Randles, C., Diehl, T., and Nielsen, E.: Influence of the 2006 Indonesian biomass burning aerosols on tropical dynamics studied with the GEOS5 AGCM, *J. Geophys. Res.*, 115, D14121, doi:10.1029/2009JD013181, 2010.
- Patra, P. K., Houweling, S., Krol, M., Bousquet, P., Belikov, D., Bergmann, D., Bian, H., Cameron-Smith, P., Chipperfield, M. P., Corbin, K., Fortems-Cheiney, A., Fraser, A., Gloor, E., Hess, P., Ito, A., Kawa, S. R., Law, R. M., Loh, Z., Maksyutov, S., Meng, L., Palmer, P. I., Prinn, R. G., Rigby, M., Saito, R., and Wilson, C.: TransCom model simulations of CH₄ and related species: linking transport, surface flux and chemical loss with CH₄ variability in the troposphere and lower stratosphere, *Atmos. Chem. Phys.*, 11, 12813–12837, doi:10.5194/acp-11-12813-2011, 2011.
- Patra, P. K., Krol, M. C., Montzka, S. A., Arnold, T., Atlas, E. L., Lintner, B. R., Xiang, B., Elkins, J. W., Fraser, P. J., Ghosh, A., Hints, E. J., Hurst, D. F., Ishijima, K., Krummel, P. B., Miller, B. R., Miyazaki, K., Moore, F. L., Mühle, J., O'Doherty, S., Prinn, R. G., Steele, L. P., Takigawa, M., Wang, H. J., Weiss, R. F., Wofsy, S. C., and Young, D.: Observational evidence for

- interhemispheric hydroxyl-radical parity, *Nature*, 513, 219–223, doi:10.1038/nature13721, 2014.
- Pawson, S. R., Stolarski, S., Douglass, A. R., Newman, P. A., Nielsen, J. E., Frith, S. M., and Gupta, M. L.: Goddard Earth Observing System chemistry-climate model simulations of stratospheric ozone-temperature coupling between 1950 and 2005, *J. Geophys. Res.*, 113, D12103, doi:10.1029/2007JD009511, 2008.
- Prather, M.: Lifetimes and Eigen states in atmospheric chemistry, *Geophys. Res. Lett.*, 21, 801–804, 1994.
- Prather, M.: Time scales in atmospheric chemistry: Theory, GWPs for CH₄ and CO, and runaway growth, *Geophys. Res. Lett.*, 23, 2597–2600, doi:10.1029/96GL02371, 1996.
- Prather, M. and Spivakovsky, C. M.: Tropospheric OH and the lifetimes of hydrochlorofluorocarbons, *J. Geophys. Res.*, 95, 18723–18729, doi:10.1029/JD095iD11p18723, 1990.
- Prather, M. J., Holmes, C. D., and Hsu, J.: Reactive greenhouse gas scenarios: Systematic exploration of uncertainties and the role of atmospheric chemistry, *Geophys. Res. Lett.*, 39, L09803, doi:10.1029/2012GL051440, 2012.
- Prinn, R. G., Huang, J., Weiss, R. F., Cunnold, D. M., Fraser, P. J., Simmonds, P. G., McCulloch, A., Harth, C., Reimann, S., Salameh, P., O'Doherty, S., Wang, R. H. J., Porter, L. W., Miller, B. R., and Krummel, P. B.: Evidence for variability of atmospheric hydroxyl radicals over the past quarter century, *Geophys. Res. Lett.*, 32, L07809, doi:10.1029/2004GL022228, 2005.
- Randerson, J. T., van der Werf, G. R., Giglio, L., Collatz, G. J., and Kasibhatl, P. S.: Global Fire Emissions Database, Version 3 (GFEDv3.1), Data set, Oak Ridge National Laboratory Distributed Active Archive Center, Oak Ridge, Tennessee, USA, available at: <http://daac.ornl.gov> (last access: 27 October 2015), doi:10.3334/ORNLDAAAC/1191, 2013.
- Rienecker, M. M., Suarez, M. J., Todling, R., Bacmeister, J., Takacs, L., Liu, H.-C., Gu, W., Sienkiewicz, M., Koster, R. D., Gelaro, R., Stajner, I., and Nielsen, J. E.: The GEOS-5 data assimilation system – Documentation of Versions 5.0.1, 5.1.0, and 5.2.0, Technical Report Series on Global Modeling and Data Assimilation, Vol. 27, available at: http://gmao.gsfc.nasa.gov/pubs/docs/GEOS5_104606-Vol27.pdf (last access: 27 October 2015), 2008.
- Rohrer, F. and Berresheim, H.: Strong correlations between levels of tropospheric hydroxyl radicals and solar ultraviolet radiation, *Nature*, 442, 184–187, doi:10.1038/nature04924, 2006.
- Rohrer, F., Lu, K., Hofzumahaus, A., Bohn, B., Brauers, T., Chang, C.-C., Fuchs, H., Häseler, R., Holland, F., Hu, M., Kita, K., Kondo, Y., Li, X., Lou, S., Oebel, A., Shao, M., Zeng, L., Zhu, T., Zhang, Y., and Wahner, A.: Maximum efficiency in the hydroxyl-radical-based self-cleansing of the troposphere, *Nat. Geosci.* 7, 559–563, doi:10.1038/ngeo2199, 2014.
- Sander, S. P., Abbatt, J., Barker, J. R., Burkholder, J. B., Friedl, R. R., Golden, D. M., Huie, R. E., Kolb, C. E., Kurylo, M. J., Moortgat, G. K., Orkin, V. L., and Wine, P. H.: Chemical Kinetics and Photochemical Data for Use in Atmospheric Studies, Evaluation No. 17, JPL Publication 10-6, Jet Propulsion Laboratory, Pasadena, available at: <http://jpldataeval.jpl.nasa.gov> (last access: 27 October 2015), 2011.
- Schneising, O., Buchwitz, M., Burrows, J. P., Bovensmann, H., Bergamaschi, P., and Peters, W.: Three years of greenhouse gas column-averaged dry air mole fractions retrieved from satellite – Part 2: Methane, *Atmos. Chem. Phys.*, 9, 443–465, doi:10.5194/acp-9-443-2009, 2009.
- Schneising, O., Buchwitz, M., Reuter, M., Heymann, J., Bovensmann, H., and Burrows, J. P.: Long-term analysis of carbon dioxide and methane column-averaged mole fractions retrieved from SCIAMACHY, *Atmos. Chem. Phys.*, 11, 2863–2880, doi:10.5194/acp-11-2863-2011, 2011.
- Schultz, M., Rast, S., van het Bolscher, M., Pulles, T., Brand, R., Pereira, J., Mota, B., Spessa, A., Dalsøren, S., van Noije, T., and Szopa, S.: Emission data sets and methodologies for estimating emissions, RETRO project report D1-6, Hamburg, 26 February 2007, available at: http://gcmd.gsfc.nasa.gov/records/GCMD_GEIA_RETRO.html (last access: 27 October 2015), 2007.
- Shindell, D. T., Faluvegi, G., Stevenson, D. S., Krol, M. C., Emmons, L. K., Lamarque, J.-F., Petron, G., Dentener, F. J., Ellingsne, K., Schultz, M. G., Wild, O., Amann, M., Atherton, C. S., Bergmann, D. J., Bey, I., Butler, T., Cofala, J., Collins, W. J., Derwent, R. G., Doherty, R. M., Drevet, J., Eskes, H. J., Fiore, A. M., Gauss, M., Hauglustaine, D. A., Horowitz, L. W., Isaksen, I. S. A., Lawrence, M. G., Montanaro, V., Müller, J.-F., Pitari, G., Prather, M. J., Pyle, J. A., Rast, S., Rodriguez, J. M., Sanderson, M. G., Savage, N. H., Strahan, S. E., Sudo, K., Szopa, S., Unger, N., van Noije, T. P. C., and Zeng, G.: Multimodel simulations of carbon monoxide: Comparison with observations and projected near-future changes, *J. Geophys. Res.*, 111, D19306, doi:10.1029/2006JD007100, 2006.
- Spivakovsky, C., Wofsy, S., and Prather, M.: A numerical method for the parameterization of atmospheric chemistry: Computation of tropospheric OH, *J. Geophys. Res.*, 95, 18433–18439, 1990a.
- Spivakovsky, C. M., Yevich, R., Logan, J. A., Wofsy, S. C., McElroy, M. B., and Prather, M. J.: Tropospheric OH in a three-dimensional chemical tracer model: An assessment based on observations of CH₃CCl₃, *J. Geophys. Res.*, 95, 18441–18471, doi:10.1029/JD095iD11p18441, 1990b.
- Spivakovsky, C. M., Logan, J. A., Montzka, S. A., Balkanski, Y. J., Foreman-Fowler, M., Jones, D. B. A., Horowitz, L. W., Fusco, A. C., Brenninkmeijer, C. A. M., Prather, M. J., Wofsy, S. C., and McElroy, M. B.: Three-dimensional climatological distribution of tropospheric OH: Update and evaluation, *J. Geophys. Res.*, 105, 8931–8980, doi:10.1029/1999JD901006, 2000.
- Stone, D., Whalley, L. K., and Heard, D. E.: Tropospheric OH and HO₂ radicals: field measurements and model comparisons, *Chem. Soc. Rev.*, 41, 6348, doi:10.1039/c2cs35140d, 2012.
- Strahan, S. E., Duncan, B. N., and Hoor, P.: Observationally derived transport diagnostics for the lowermost stratosphere and their application to the GMI chemistry and transport model, *Atmos. Chem. Phys.*, 7, 2435–2445, doi:10.5194/acp-7-2435-2007, 2007.
- Strode, S. A., Duncan, B. N., Yegorova, E. A., Kouatchou, J., Ziemke, J. R., and Douglass, A. R.: Implications of carbon monoxide bias for methane lifetime and atmospheric composition in chemistry climate models, *Atmos. Chem. Phys.*, 15, 11789–11805, doi:10.5194/acp-15-11789-2015, 2015.
- Voulgarakis, A., Naik, V., Lamarque, J.-F., Shindell, D. T., Young, P. J., Prather, M. J., Wild, O., Field, R. D., Bergmann, D., Cameron-Smith, P., Cionni, I., Collins, W. J., Dalsøren, S. B., Doherty, R. M., Eyring, V., Faluvegi, G., Folberth, G. A., Horowitz, L. W., Josse, B., MacKenzie, I. A., Nagashima, T., Plummer, D. A., Righi, M., Rumbold, S. T., Stevenson, D. S., Strode, S. A., Sudo, K., Szopa, S., and Zeng, G.: Analysis of present day and

- future OH and methane lifetime in the ACCMIP simulations, *Atmos. Chem. Phys.*, 13, 2563–2587, doi:10.5194/acp-13-2563-2013, 2013.
- Voulgarakis, A., Marlier, M. E., Faluvegi, G., Shindell, D. T., Tsigaridis, K., and Mangeon, S.: Interannual variability of tropospheric trace gases and aerosols: The role of biomass burning emissions, *J. Geophys. Res. Atmos.*, 120, 7157–7173, doi:10.1002/2014JD022926, 2015.
- Wang, J. S., Logan, J. A., McElroy, M. B., Duncan, B. N., Megretskaia, I. A., and Yantosca, R. M.: A 3-D model analysis of the slowdown and interannual variability in the methane growth rate from 1988 to 1997, *Global Biogeochem. Cy.*, 18, GB3011, doi:10.1029/2003GB002180, 2004.
- Wang, J. S., McElroy, M. B., Logan, J. A., Palmer, P. I., Chameides, W. L., Wang, Y., and Megretskaia, I. A.: A quantitative assessment of uncertainties affecting estimates of global mean OH derived from methyl chloroform observations, *J. Geophys. Res.*, 113, D12302, doi:10.1029/2007JD008496, 2008.
- Wild, O. and Palmer, P. I.: How sensitive is tropospheric oxidation to anthropogenic emissions?, *Geophys. Res. Lett.*, 35, L22802, doi:10.1029/2008GL035718, 2008.
- Wolter, K. and Timlin, M. S.: El Niño/Southern Oscillation behaviour since 1871 as diagnosed in an extended multivariate ENSO index (MEI.ext), *Int. J. Climatol.*, 31, 1074–1087, doi:10.1002/joc.2336, 2011.
- Worden, H. M., Deeter, M. N., Edwards, D. P., Gille, J. C., Drummond, J. R., and Nédélec, P.: Observations of near-surface carbon monoxide from space using MOPITT multispectral retrievals, *J. Geophys. Res.*, 115, D18314, doi:10.1029/2010JD014242, 2010.